UNIVERSITY *of York*

This is a repository copy of *A family of dual-activity glycosyltransferasesphosphorylases mediates mannogen turnover and virulence in Leishmania parasites*.

White Rose Research Online URL for this paper:
https://eprints.whiterose.ac.uk/id/eprint/149916/

Version: Published Version

Article:

White Rose
university consortium
Universities of Leeds, Sheffield & York

eprints@whiterose.ac.uk
https://eprints.whiterose.ac.uk/

Cell Host & Microbe

A Family of Dual-Activity Glycosyltransferase-Phosphorylases Mediates Mannogen Turnover and Virulence in *Leishmania* Parasites

Graphical Abstract
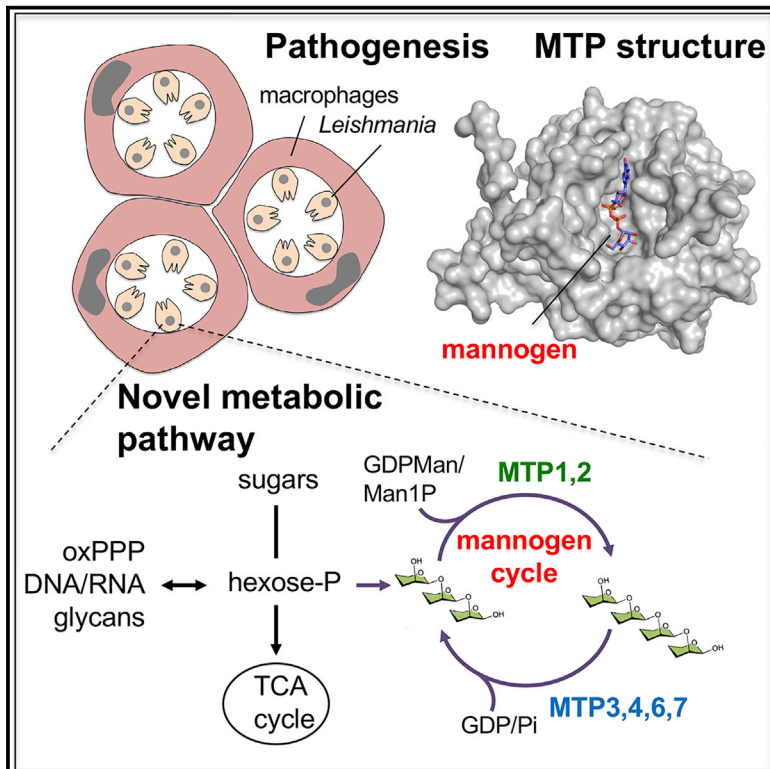
Authors

M. Fleur Sernee, Julie E. Ralton, Tracy L. Nero, ..., Spencer J. Williams, Gideon J. Davies, Malcolm J. McConville

Correspondence

malcolmm@unimelb.edu.au

In Brief

Sernee et al. show that metabolism of the *Leishmania* carbohydrate reserve, mannogen, is mediated by a single family of enzymes acquired by horizontal gene transfer. The evolution of this pathway may have allowed these parasites to expand their host range and colonize intracellular niches in their vertebrate hosts.

Highlights

- *Leishmania* have replaced canonical carbohydrate reserves with mannogen

- Mannogen cycling is regulated by dual-activity sugar transferase/phosphorylases

- Enzyme evolution required horizontal gene transfer and enzyme substrate diversification

- Mannogen cycling protects against glucose toxicity and is essential for virulence

CellPress

CellPress

A Family of Dual-Activity Glycosyltransferase-Phosphorylases Mediates Mannogen Turnover and Virulence in *Leishmania* Parasites

M. Fleur Sernee,[1,6] Julie E. Ralton,[1,6] Tracy L. Nero,[1,2] Lukasz F. Sobala,[3] Joachim Kloehn,[1] Marcel A. Vieira-Lara,[1] Simon A. Cobbold,[1] Lauren Stanton,[1] Douglas E.V. Pires,[1] Eric Hanssen,[1,4] Alexandra Males,[3] Tom Ward,[3] Laurence M. Bastidas,[3] Phillip L. van der Peet,[5] Michael W. Parker,[1,2] David B. Ascher,[1] Spencer J. Williams,[5] Gideon J. Davies,[3] and Malcolm J. McConville[1,7,*]

[1]Department of Biochemistry and Molecular Biology, Bio21 Molecular Science and Biotechnology Institute, University of Melbourne, Parkville, VIC 3010, Australia
[2]ACRF Rational Drug Discovery Centre, St. Vincent's Institute of Medical Research, Fitzroy, VIC 3065, Australia
[3]Department of Chemistry, University of York, York YO10 5DD, UK
[4]Advanced Microscopy Facility, Bio21 Molecular Science and Biotechnology Institute, University of Melbourne, Parkville, VIC 3010, Australia
[5]School of Chemistry, Bio21 Molecular Science and Biotechnology Institute, University of Melbourne, Parkville, VIC 3010, Australia
[6]These authors contributed equally
[7]Lead Contact
*Correspondence: malcolmm@unimelb.edu.au
https://doi.org/10.1016/j.chom.2019.08.009

SUMMARY

Parasitic protists belonging to the genus *Leishmania* synthesize the non-canonical carbohydrate reserve, mannogen, which is composed of β-1,2-mannan oligosaccharides. Here, we identify a class of dual-activity mannosyltransferase/phosphorylases (MTPs) that catalyze both the sugar nucleotide-dependent biosynthesis and phosphorolytic turnover of mannogen. Structural and phylogenic analysis shows that while the MTPs are structurally related to bacterial mannan phosphorylases, they constitute a distinct family of glycosyltransferases (GT108) that have likely been acquired by horizontal gene transfer from gram-positive bacteria. The seven MTPs catalyze the constitutive synthesis and turnover of mannogen. This metabolic rheostat protects obligate intracellular parasite stages from nutrient excess, and is essential for thermotolerance and parasite infectivity in the mammalian host. Our results suggest that the acquisition and expansion of the MTP family in *Leishmania* increased the metabolic flexibility of these protists and contributed to their capacity to colonize new host niches.

INTRODUCTION

The Trypanosomatidae are parasitic protists that cause diseases such as human African trypanosomiasis (*Trypanosoma brucei*), Chagas disease (*T. cruzi*), and human leishmaniasis (*Leishmania spp*) that are estimated to chronically or acutely infect more than 100 million people worldwide (Stuart et al., 2008; Singh et al., 2014; Burza et al., 2018; Bañuls et al., 2011). These pathogens often have complex life cycles, occu-

pying extracellular and intracellular niches in different insect, plant, and vertebrate hosts. Comparative analyses of the genomes of these parasites and related free-living protists indicate that the evolution of parasitic lifestyles has been associated with loss of metabolic pathways and genome reduction, as well as the acquisition of lineage-specific innovations, that have contributed to parasite survival in different host niches (Jackson et al., 2016; Opperdoes et al., 2016). The absence of canonical reserve poly- or oligosaccharides (e.g., glycogen, starch, sucrose, trehalose) in the trypanosomatids constitutes a particularly dramatic example of metabolic pathway loss. The dynamic synthesis and turnover of carbohydrate reserves in other eukaryotes plays a key role in regulating central carbon metabolism and cellular stress responses (François and Parrou, 2001; Shi et al., 2010; MacNeill et al., 2017), suggesting that early trypanosomatids may have developed compensatory mechanisms for dealing with variable nutrient levels and other environmental stresses (Jackson et al., 2016). Intriguingly, *Leishmania* and closely related trypanosomatids (including the plant pathogen *Phytomonas* and insect parasites *Leptomonas*, *Crithidia*, and *Herpetomonas*) have subsequently acquired a new pathway of carbohydrate reserve biosynthesis (Ralton et al., 2003; Sernee et al., 2006). These parasites synthesize mannogen, a family of linear oligosaccharides made up of 2-60 β-1,2-linked mannose residues (Previato et al., 1984; Keegan and Blum, 1992; Ralton et al., 2003). The absence of mannogen in the *Trypanosoma* suggests that this pathway evolved following the separation of these different trypanosomatid lineages. How the acquisition of mannogen synthesis contributes to the parasitic lifestyle of *Leishmania* remains unclear.

Mannogen accumulates to very high levels (>10 mM) in pathogenic stages of *Leishmania* (Ralton et al., 2003). These include the non-dividing promastigote stages that develop in the foregut of the sandfly vector and initiate infection in the mammalian host and the obligate intracellular amastigote stages that colonize the phagolysosome of macrophages and other phagocytic cells in the mammalian host and perpetuate both acute and long-term
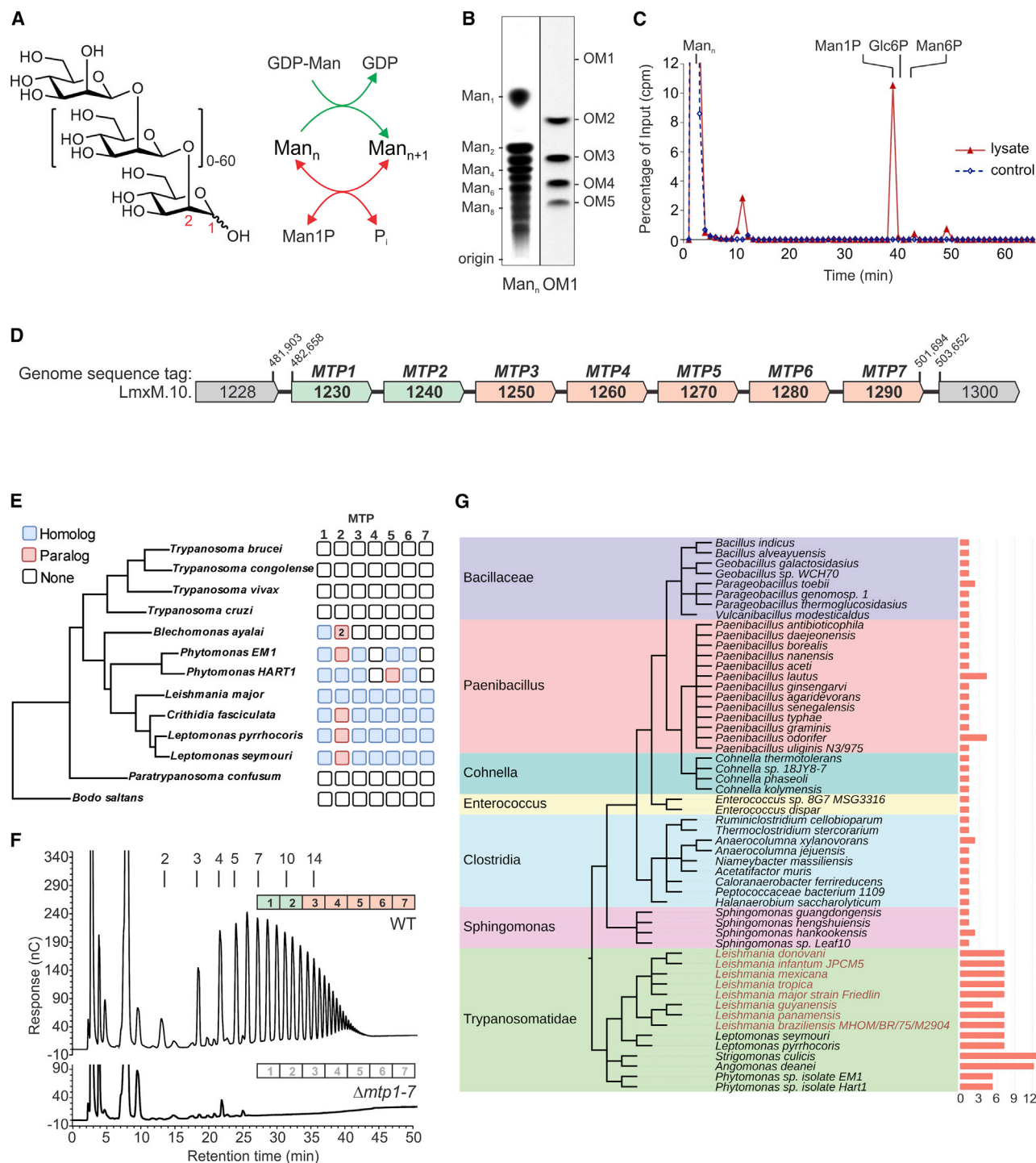
Figure 1. Identification of a *Leishmania* Gene Family Required for Mannogen Synthesis

(A) Putative role of GDP-Man-dependent transferase(s) and glycan phosphorylase(s) in mannogen cycling.

(B) HPTLC separation of ^{3}H-mannogen (DP 2–10) or octyl-^{3}H-mannogen (DP 1–5) oligomers generated by incubation of *L. mexicana* Δ*gmp* cell-free lysates with GDP-^{3}H-Man and purified mannogen (Man$_n$) or the synthetic mannose acceptor OM1.

(C) HPAEC detection of ^{3}H-Man1P released after incubation of *L. mexicana* Δ*pmm* cell-free lysates (and boiled control) with ^{3}H-mannogen (Man$_n$).

(D) The *L. mexicana* MTP1-7 gene array on chromosome 10.

(legend continued on next page)

chronic infections in humans. While the enzymes involved in mannogen synthesis and turnover have yet to be identified, biochemical studies suggest that mannogen oligosaccharides are initially assembled on a mannose phosphate primer and subsequently extended by guanosine diphosphate (GDP)-Man-dependent mannosyltransferases (Sernee et al., 2006; van der Peet et al., 2006). Conversely, the rapid degradation of mannogen under glucose-limiting conditions (Ralton et al., 2003) implies the presence of putative mannosidases (which remove neutral sugars or disaccharides from the non-reducing termini of glycans) or glycan phosphorylases (which remove sugar-1-phosphates that can feed directly into central carbon metabolism without consumption of ATP) (Figure 1A). Significantly, *Leishmania* mutants lacking key enzymes in GDP-Man synthesis have global defects in mannogen synthesis, as well as protein and lipid mannosylation (Ralton et al., 2003), and are avirulent in animal models (Garami and Ilg, 2001), suggesting that one or more of these pathways is important for virulence.

Here, we show that mannogen synthesis and turnover is regulated by a single family of glycosyltransferases that, uniquely, exhibit dual sugar-nucleotide-dependent mannosyltransferase and glycan phosphorylase activities. Analysis of the structure and function of these enzymes suggests that the mannogen pathway evolved through a process of horizontal gene transfer (HGT), gene duplication, and expanded substrate promiscuity. We show that the synthesis and turnover of mannogen regulates *Leishmania* central carbon metabolism and cellular stress responses under both nutrient replete, as well as nutrient-limiting conditions, and is essential for parasite infectivity in the mammalian host. The evolution of this pathway may therefore have played a pivotal role in enabling these parasites to colonize new insect and mammalian host niches.

RESULTS

Detection of Mannogen Synthase and Phosphorylase Activities in *Leishmania* Extracts

In support of earlier studies (Ralton et al., 2003; van der Peet et al., 2006, 2012), mannogen synthesis was shown to be mediated by GDP-Man-dependent mannosyltransferase(s), as incubation of *L. mexicana* cell-free extracts with GDP-^{3}H-Man and either native mannogen or the synthetic substrate, octyl-α-D-mannopyranoside (OM1), resulted in the synthesis of labeled oligosaccharides (Figure 1B) comprising linear chains of β-1,2-linked mannose (Figures S1A and S1B). Competition experiments showed that OM1 was elongated by the same mannosyltransferases that elongate native mannogen (Figure S1C), while short pulse-labeling of live parasites with ^{3}H-mannose, followed by subcellular fractionation, showed that mannogen synthesis occurs primarily in the cytoplasm (Figure S1D).

To assess whether mannogen turnover is regulated by mannosidases (exo or endo) or a glycan phosphorylase, cell lysates were prepared from *L. mexicana Δpmm* promastigotes and

incubated with ^{3}H-mannogen. This parasite line lacks the enzyme phosphomannnomutase, preventing the catabolism of any mannose-1-phosphate (Man1P) generated in these assays. A single labeled product was generated that co-eluted with authentic Man1P on high-pH anion exchange chromatography (HPAEC) (Figure 1C). Free [^{3}H]-mannose or manno-oligosaccharides were not generated in these assays, indicating that mannogen turnover is primarily mediated by a glycan phosphorylase.

Identification of a Gene Family in *Leishmania* encoding Putative Mannoside Phosphorylases

Bioinformatic searches of the *Leishmania* genomes revealed a tandem array of seven genes on chromosome 10 (Figure 1D) that shared 45%–68% sequence identity with each other and distant sequence homology (5%–12% identity) to β-1,2-, β-1,3-, and β-1,4-mannosidases or phosphorylases belonging to the carbohydrate active enzyme (CAZy) family 130 glycoside hydrolases (Cuskin et al., 2015; Senoura et al., 2011; Lombard et al., 2014; Ye et al., 2016; Saburi, 2016) (Figures S2A and S3). Related gene arrays, containing between 2 and 12 genes, were also present in closely related trypanosomatids (e.g., *Phytomonas* spp, *C. fasciculata, Leptomonas* spp) that synthesize mannogen, but not in more distantly related trypanosomatids (e.g., *T. cruzi, T. brucei*) that lack any storage carbohydrates (Figure 1E). Interestingly, the crystal structure of one of the proteins encoded by the *L. major* gene array (hypothetical *L. major* protein encoded by LmjF.10.1260; PDB: 2B4W) has been deposited and shown to have the same five-bladed β-propeller fold as the bacterial GH130 proteins. To assess the function of this gene family and its role in mannogen catabolism, a *L. mexicana* null mutant lacking the entire seven gene array was generated by replacement of the diploid chromosomal loci with bleomycin drug-resistance cassettes. Unexpectedly, the mutant promastigotes, which grew normally in rich medium, were found to be completely deficient in mannogen (Figure 1F), indicating that the encoded proteins may have a role in mannogen biosynthesis in addition to, or instead of, their predicted catabolic role. Based on the genetic and biochemical studies described below, the encoded *Leishmania* proteins have been termed mannosyltransferase/phosphorylases (MTPs) and assigned to a new CAZy family of glycosyltransferases, GT108.

Phylogenetic Analysis of Family GT108

Phylogenetic analysis indicated that the *Leishmania MTP* gene array was acquired after the split that gave rise to the Trypanosomatidae (*Typanosoma* spp) and the subfamily Leishmaniinae (comprising the genera *Leishmania, Phytomonas, Leptomonas, Crithidia*, and *Blechomonas*) (Figures 1E and S2). The absence of GT108 homologs in free-living *Bodo saltans* and *Paratrypanosoma confusum* indicates that the lack of GT108 homologs in *Trypanosoma* spp is not due to recent loss in these lineages. The earliest branches of the Leishmaniinae, *B. ayalai* and

(E) Distribution of MTP homologs and paralogs in different kinetoplastid lineages. Homologs and paralogs are defined based upon their distribution within the phylogenetic tree. *B. ayalai* contains two paralogs of MTP2.
(F) HPAEC analysis of mannogen levels in *L. mexicana* wild-type (WT) and *Δmtp1-7* promastigotes. The DP of mannogen oligomers are indicated.
(G) Distribution of GT108 members in different gram-positive bacterial and trypanosomatid taxa (GT108 gene copy number is indicated in the side bar).
See also Figures S1–S3 and Tables S4 and S5.

Phytomonas spp, contain two and five GT108 homologs or paralogs, respectively, suggesting that the primordial mannogen pathway may have required just two GT108 genes and that these loci have subsequently undergone several rounds of duplication in other members of this subfamily (Figure 1E).

tBLASTN searches of the non-redundant protein sequence and TriTrypDB databases using the *Leishmania* GT108 sequences as a query led to the identification of >100 sequences of bacterial origin filtered based on e-value (<1e^{-50}) (Figures 1G, S2A, and S2B). No eukaryotic sequences were identified outside the trypanosomatids (Figures 1G and S2B). Most of the bacterial GT108 family members were associated with sequenced and annotated genomes of gram-positive bacteria belonging to the phylum Firmicutes and are annotated as hypothetical proteins with unknown function (Figure 1G). Several of these genera are present in the gut microbiota (e.g., *Paenibacillus*) of trypanosomatid insect vectors (Dey et al., 2018), suggesting that the GT108 genes may have been acquired by horizontal gene transfer in this host niche.

Several *Leishmania* MTPs Exhibit β-1,2-Mannoside Phosphorylase Activity

The seven *L. mexicana* proteins were expressed in *E. coli* and recombinant proteins incubated with the β-1,2-mannan acceptor, OM4, together with either 1 mM phosphate (Pi) or Man1P, to assess their phosphorolytic and reverse phosphorolytic (biosynthetic) activities, respectively (Figure 2A) (Kitaoka, 2015). MTP3, 4, 6, and 7 exhibited strong phosphorolytic activity, catalyzing the degradation of OM4 to OM1–3 in the presence of Pi (Figure 2B) with production of Man1P (Figure 2C). No activity was observed in the absence of Pi, indicating that the MTPs lack β-mannosidase activity. Conversely, incubation of MTP3, 4, 6, and 7 with Man1P instead of Pi resulted in elongation of OM4 (Figure 2B) and release of Pi (Figure S1E). The forward and reverse phosphorolytic activity of these enzymes did not require the divalent cations, Mn^{2+} or Mg^{2+} (Figure S1F). MTP3 and MTP6 could generate long mannogen chains (degree of polymerization [DP] >16) by reverse phosphorolysis, while MTP4 and 7 generated shorter mannooligosaccharides (DP 1–12) at equilibrium (Figure 2B). In contrast, recombinant MTP1, 2, and 5 proteins lacked detectable forward or reverse phosphorolytic activity in these assays (Figure 2B).

The *Leishmania* MTPs Exhibit Dual Phosphorolytic and Mannosyltransferase Activities

To investigate whether the MTPs are also responsible for the GDP-Man-dependent mannosyltransferase activity detected in cell lysates (Figure 1B), recombinant MTP proteins were incubated with OM4 (or OM1) and GDP-Man (Figures 2D, 2E, S1G, and S1H). Strikingly, both MTP1 and MTP2 extended these primers in the presence of GDP-Man, generating either highly extended octyl-mannogen chains (DP 5 to >30) or a family of shorter octyl-mannogen oligomers (DP 2–8) (Figures 2D and S1H). The GDP-Man-dependent mannosyltransferase activities of MTP1 and 2 are reversible, as indicated by the trimming of the OM4 substrate in the presence of GDP-Man or GDP (Figures 2D and 2F) and detection of GDP-Man synthesis in the presence of GDP (Figure S1I).

MTP3, 4, 6, and 7 could also elongate the synthetic acceptor, OM1, with a single β-1,2-mannose residue in the presence of

GDP-Man (Figure S4A). However, they could not elongate OM4 but instead generated new products that co-migrated with mannose (Man$_1$), Manβ1-2Man (Man$_2$), and Manβ1-2Manβ1-2Man (Man$_3$) (Figure 2D). These observations suggest that GDP-Man is cleaved by these MTPs in the absence of suitable acceptor to generate free mannose that acts as an alternative primer of β-1,2-mannose oligosaccharide synthesis. Interestingly, MTP4 and 6 (but not MTP3, 5, and 7) generated a mixed series of octyl-mannogen oligomers when incubated with OM4 and GDP (Figure 2D), consistent with the finding that they can catalyze synthesis of GDP-Man (Figure S1I). The fact that GDP was more effective than GDP-Man in promoting MTP4- and MTP6-dependent elongation of OM4 indicates that the newly synthesized GDP-Man remains bound to the catalytic –1 subsite, while an acceptor glycan enters the +1 subsite, allowing net elongation of the oligomannoside pool.

Co-incubation of MTP3, 4, and 6 with both GDP-Man and Man1P enhanced OM1 elongation, indicating that both donors are accommodated within the same active site. Consistent with this conclusion, incubation of MTP4 with OM1 (1 mM), GDP-^{3}H-Man (50 μM) and increasing concentrations of α-Man1P (50 μM to 5 mM) competitively inhibited GDP-^{3}H-Man incorporation (Figure 2G). In contrast, β-Man1P only competed with GDP-^{3}H-Man when added at 100-fold excess (reflecting the fact that this sugar can also act as an acceptor). α-Man1P and GDP-Man may therefore compete for the same mannose donor (–1) subsite in these enzymes.

These data show that MTP1 and 2 function primarily as GDP-Man-dependent β-1,2-mannosyltransferases, while MTP3, 4, 6, and 7 act as β-1,2-mannooligosaccharide phosphorylases with dual transferase activity. MTP5 lacks detectable activity in all of these assays, and the function of this protein remains unknown (Figures 2B and 2D).

Identification of Catalytic Site Residues Responsible for Phosphorolytic and Mannosyltransferase Activities

To better understand the dual transferase and phosphorylase activities of this enzyme family, the 3D structures of MTP1, MTP2, and MTP4 containing different substrates were determined (Figures 3A–3C, S5, and S6; Tables S1 and S2). Like the deposited structure of the *L. major* MTP4 protein (PDB: 2B4W), all three proteins adopt a five-bladed β-propeller fold, with each blade composed of a β sheet with three or four antiparallel strands surrounding an extended central pocket comprising the active site (Figures 3A–3C). The catalytic pockets of these proteins have similar architecture to those of the sequence-divergent bacterial CAZy family GH130 proteins, such as the *Listeria innocua* β-1,2-mannobiose phosphorylase (PDB: 5B0R) (Tsuda et al., 2015) (Figure 3E). In particular, overlay of the catalytic pocket of MTP4 and the *L. innocua* protein revealed equivalent Pi coordinating residues (Arg150, His208, Asp134, and Tyr224; numbering for *L. mexicana* MTP4) arranged identically in space (Figure 3E; Table S2). Similarly, the identity, spatial arrangement, and interactions of residues in the –1 mannosyl transfer site are identical. These include the Phe265 aromatic platform and residues that interact with different hydroxyls of the –1 mannose, such as Lys133 with mannose C(O)2, Asp83 with mannose C(O)3 (proposed catalytic acid/base in the reaction mechanism; see below), Asn32 with mannose C(O)4, and Asp285 with mannose C(O)6
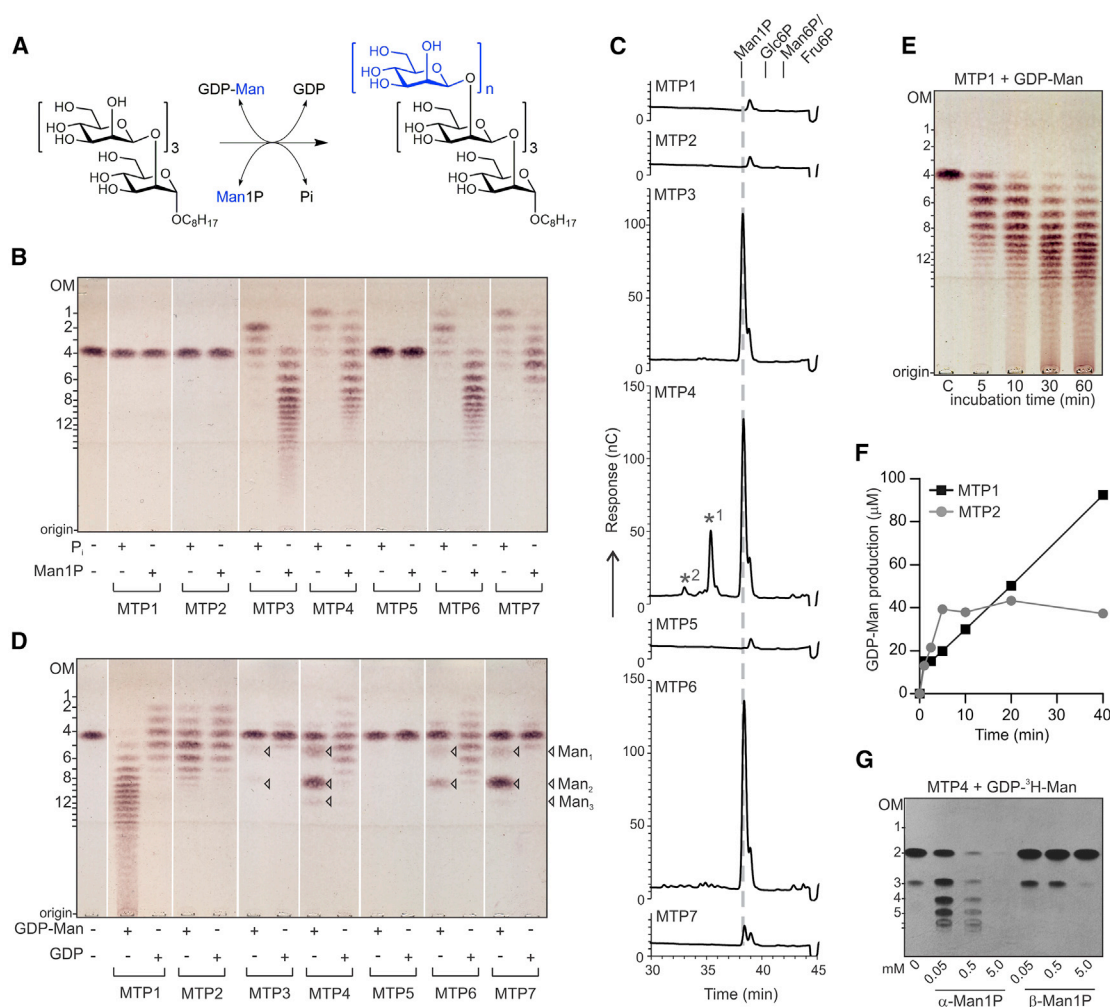
Figure 2. The *Leishmania* MTPs Exhibit Dual Mannosyltransferase and Phosphorylase Activities

(A) Enzyme assays used to measure MTP mannosyltransferase and reverse phosphorolytic activity.

(B) HPTLC separation of octyl-mannogen oligosaccharides (DP 1–16) generated by incubation of MTP proteins with OM4 and either Pi or Man1P.

(C) HPAEC separation of Man1P and phosphooligosaccharides (*) synthesized by MTP proteins incubated with mannogen and Pi. MTP4 synthesized Man-β-1,2-Manα-P (*[1]) and [Manβ-1,2]$_2$-Manα-P (*[2]), in addition to Man1P.

(D) High-performance thin-layer chromatography (HPTLC) separation of octyl-mannogen oligosaccharides generated by incubation of MTP proteins with OM4 and either GDP-Man or GDP. Products indicated with open triangle correspond to mannose, Manβ-1,2-Manα-P (Man$_2$), and [Manβ-1,2]$_2$-Man (Man$_3$).

(E) Time-dependent synthesis of high-DP octyl-mannogen following incubation of MTP1 with OM4 and GDP-Man.

(F) Liquid chromatography-mass spectrometry (LC-MS) detection of GDP-Man synthesized by MTP1 (black squares) and MTP2 (gray dots) in the presence of octyl-mannogen (DP 1–16) and GDP.

(G) HPTLC separation of octyl-^{3}H-mannogen species synthesized by MTP4 in the presence of OM1 (1 mM) and GDP-^{3}H-Man (50 μM) and increasing concentrations of α-Man1P and β-Man1P.

See also Figures S1 and S4.

(Figures 3E and S5E). The catalytic pockets of MTP4 and the bacterial GH130 proteins also have a very similar mannose acceptor +1 subsite, where the mannose C(O)3 interacts with Arg48, C(O)4/(O)6 interacts with Glu82, and C(O)5/(O)6 interacts with Lys133 (Figures 3E, 3H, and 4A; Table S2).

The MTP1 and 2 proteins have 3D structures that are similar to MTP4 but form dimers rather than monomers in the crystal lattice and in solution (data and structure statistics in Table S1; Figures S4D, S5A, and S5B). The structure of the catalytically inactive MTP2 mutant lacking the proposed aspartate acid/base (D94N), containing β-1,2-mannobiose in the −1/+1 subsites

(Figure 3D), showed that amino acid side chains in the MTPs are spatially conserved and partake in identical interactions as the equivalent residues in the bacterial GH130 enzymes (Table S2). Neither MTP1 nor MTP2 contained canonical nucleotide binding domains despite utilizing GDP-Man as primary donor, confirming that the MTP enzymes represent a new paradigm in nucleotidyl sugar glycosyltransferases.

We were unable to obtain complexes of MTP1 and 2 with GDP or GDP-Man through co-crystallization and crystal-soaking experiments, suggesting that GDP-Man binding only occurs after binding of the mannan acceptor and/or that structural changes
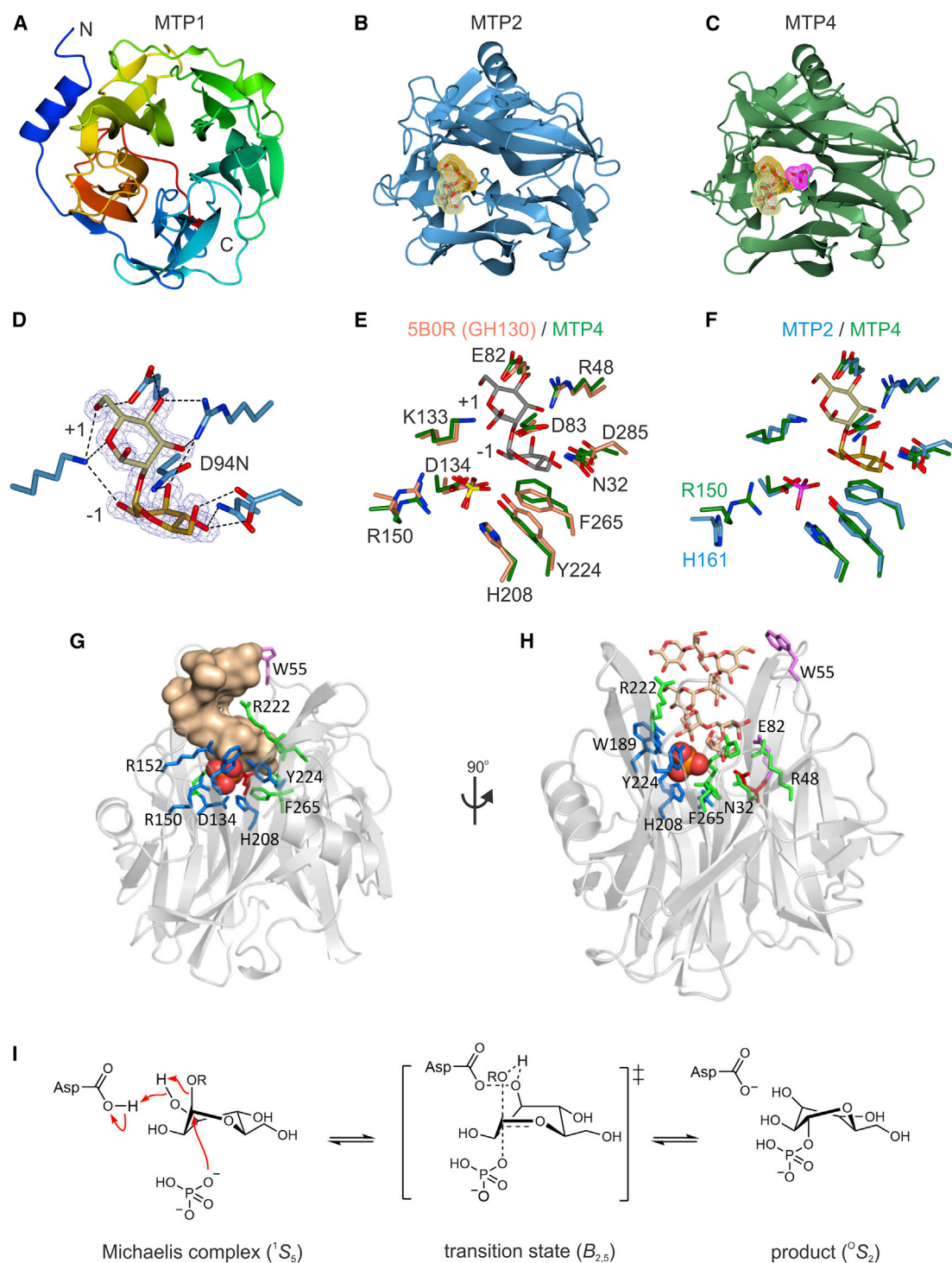
Figure 3. MTP Crystal Structures and Modeled Interactions

(A) The five-bladed β-propeller fold of MTP1 (top view). The β sheets containing three to four antiparallel strands are color coded.

(B) MTP2 (side view) with β-1,2-mannobiose (yellow stick and molecular surface representation) in the +1/−1 catalytic position. The complex was captured using the MTP2 D94N mutant and the crystal structure overlaid on native MTP2.

(C) MTP4 (side view) with the observed Pi shown in magenta. The β-1,2-mannobiose of the overlaid D94N MTP2 variant crystal complex is included for reference (D94N MTP2 protein not shown).

(D) The β-1,2-mannobiose ligand in complex with the MTP2 D94N protein.

(legend continued on next page)

may be required for nucleotide binding. Nonetheless, we could identify structural differences in the catalytic pocket of MTP1 and 2 and MTP4 that likely contribute to the different donor and acceptor specificities of these enzymes (Figures 3F, 4A, and 4C). In particular, MTP4 (and other bacterial GH130 phosphorylases) contain an Arg residue (Arg150 in MTP4) in the Pi-binding pocket, while MTP1 and 2 contain a His residue (His168 and His161, respectively) in the same position (Figures 3F, 4A, 4C, S2C, S3, and S5C–S5F; Table S2). Sequence analysis confirmed that the Arg/His switch is diagnostic for enzymes that primarily exhibit phosphorolytic versus mannosyltransferase activities, supporting the conclusion that these residues mediate critical interactions with the phosphate or GDP leaving groups, respectively (Figures S2C and S3).

Our data suggest that the MTPs have the same reaction mechanism as the bacterial GH130 phosphorylases (Nakae et al., 2013). During phosphorolysis or the reverse transferase reactions, the conserved Asp (Asp83 in MTP4, Asp94 in MTP2, Asp101 in MTP1) acts as a general acid, protonating the glycosidic leaving group via a proton relay through C(O)3, allowing phosphate to displace the anomeric glycoside leaving group (Figure 3I). Conversely, during reverse-phosphorolysis or forward-mannosyltransferase reactions, Asp83 acts as general base, deprotonating C(O)2 of a sugar nucleophile and promoting glycosidic bond formation with displacement of phosphate (or GDP) leaving group. Consistent with this mechanism, the −1 subsite mannoside is distorted into an unusual $^1S_5$ skew conformation (Figure 3I), facilitating unhindered phosphate attack and departure without steric clashes with C(O)2 (Cuskin et al., 2015).

Mutagenesis studies confirmed the importance of the active center residues in the dual phosphorolytic and mannosyltransferase activities of MTP4 (Figures 4A and 4B). Mutation of the catalytic Asp83 acid/base (D83N) resulted in complete loss of both phosphorylase and transferase activities (Figures 4A and 4B). Mutation of Lys133 (K133A, K133R) predicted to bind the OM1 acceptor in the +1 subsite of the pocket also resulted in loss of both activities. In contrast, mutations of Asp285 (D285N), which forms hydrogen bonds with C(O)4/(O)6 of the −1 subsite mannose; Asp134 (D134N), which binds the Man1P phosphate group; and Glu82 (E82A), which hydrogen bonds with C(O)4/(O)6 of the +1 sugar, led to loss of phosphorylase activity but only had minimal effect on the transferase activity. Mutation of MTP4 His208 (H208A) also had a modest effect on phosphorolysis but no effect on transferase activity. Selective retention of transferase activity indicates that the amino acid residues that interact with the GMP moiety of this donor likely assist leaving group departure.

Mutation of the conserved active center aspartate at position 94 in MTP2 (D94N) resulted in complete loss of transferase activity (Figures 4C and 4D). The active site pocket of the MTP1 and MTP2 enzymes is larger than in MTP4 and contained a His residue (His168 in MTP1 and His161 in MTP2) in place of the Arg residue in MTP4 (Arg150), which establishes hydrogen bonds with the guanine moiety of GDP-Man (Figures 4C, 4D, and S5F). The importance of the Arg/His switch was confirmed by mutating MTP2 His161 to Arg, which resulted in reduced transferase activity (Figure 4D). In contrast, mutation of MTP2 Asp145 (D145N) had little effect on transferase activity, consistent with this residue having a primary role in coordination to Man1P phosphate during phosphorolysis (Figures 4B and 4D). These data suggest that all of the MTP proteins contain a single catalytic site that preferentially accommodates either Man1P or GDP-Man as donors, together with a β-1,2-mannooligosaccharide acceptor.

Modeling of the bacterial GT108 proteins provided further support for the hypothesis that the *Leishmania* MTPs were acquired by HGT. Structural predictions of eleven bacterial GT108 proteins (Table S3) indicated that they all share the same five-bladed β-propeller fold (Figures S6A and S6B) and retain key residues in the catalytic pocket. Notably, all of the modeled bacterial proteins retained an Arg residue at the position of the Arg/His switch, indicating that they are primarily glycan phosphorylases/hydrolases (Figures S2C and S6D). *B. ayalai*, the most divergent member of the Leishmaniinae, contains three MTP genes: a homolog of MTP1 with a His residue in the Arg/His switch position and two paralogs of MTP2, which both contain Arg in the same position (Figures 1E and S2C). A functional mannogen cycle may therefore have arisen in ancestral members of the Leishmaniinae following HGT of a bacterial phosphorolytic GT108 gene and subsequent gene duplication and mutation around the Arg/His switch position to allow use of GDP-Man as donor.

Leishmania MTPs Have Non-redundant Functions In Vivo

To investigate the function of the MTPs *in vivo*, the *L. mexicana* Δ*mtp1-7* mutant was complemented with individual *MTP* genes using episome or integration vectors. Expression of MTP1 alone resulted in production of hyper-elongated mannogen oligomers (DP >60), while expression of MTP2 resulted in synthesis of a restricted pool of short mannogen oligomers (DP 2–10), consistent with the *in vitro* activities and products of each of these enzymes (Figure 5A). Co-expression of both MTP1 and 2 in the complemented *L. mexicana* Δ*mtp1–7* mutant, or targeted deletion of *MTP3–7*, resulted in an intermediate mannogen profile containing both short and long mannogen oligomers (DP 4 to >60) (Figure 5A). MTP1 and MTP2 thus appear to act cooperatively *in vivo* to regulate the synthesis of high- and low-DP pools of mannogen, respectively.

(E) Overlay of the active sites of the Pi complex of MTP4 (green) and the β-1,2-mannobiose-sulfate complex of *L. innocua* GH130 β-1,2-mannobiose phosphorylase (pink) (PDB: 5B0R) (Tsuda et al., 2015). Sulfate (yellow and red sticks) and Pi (magenta and red sticks) are co-localized; β-1,2-mannobiose in gray and red sticks.

(F) Overlay of D94N MTP2 (blue) and MTP4 (green) reveals minor changes (His or Arg residues) in the Pi site of these MTPs (Pi in magenta and red sticks and β-1,2-mannobiose in yellow and red sticks).

(G) Man$_8$ (beige molecular surface) docked into the catalytic site of MTP4 (semi-transparent cartoon). Residues in the Pi site and +1/−1 acceptor and donor subsites shown as sticks (colored according to their location as defined in Figure S3 and Table S2); Pi depicted as spheres.

(H) View is a 90° rotation about the y axis to that shown in (G). Man$_8$ depicted as thin sticks (beige and red).

(I) Canonical catalytic mechanism for GH130 and MTP enzymes.

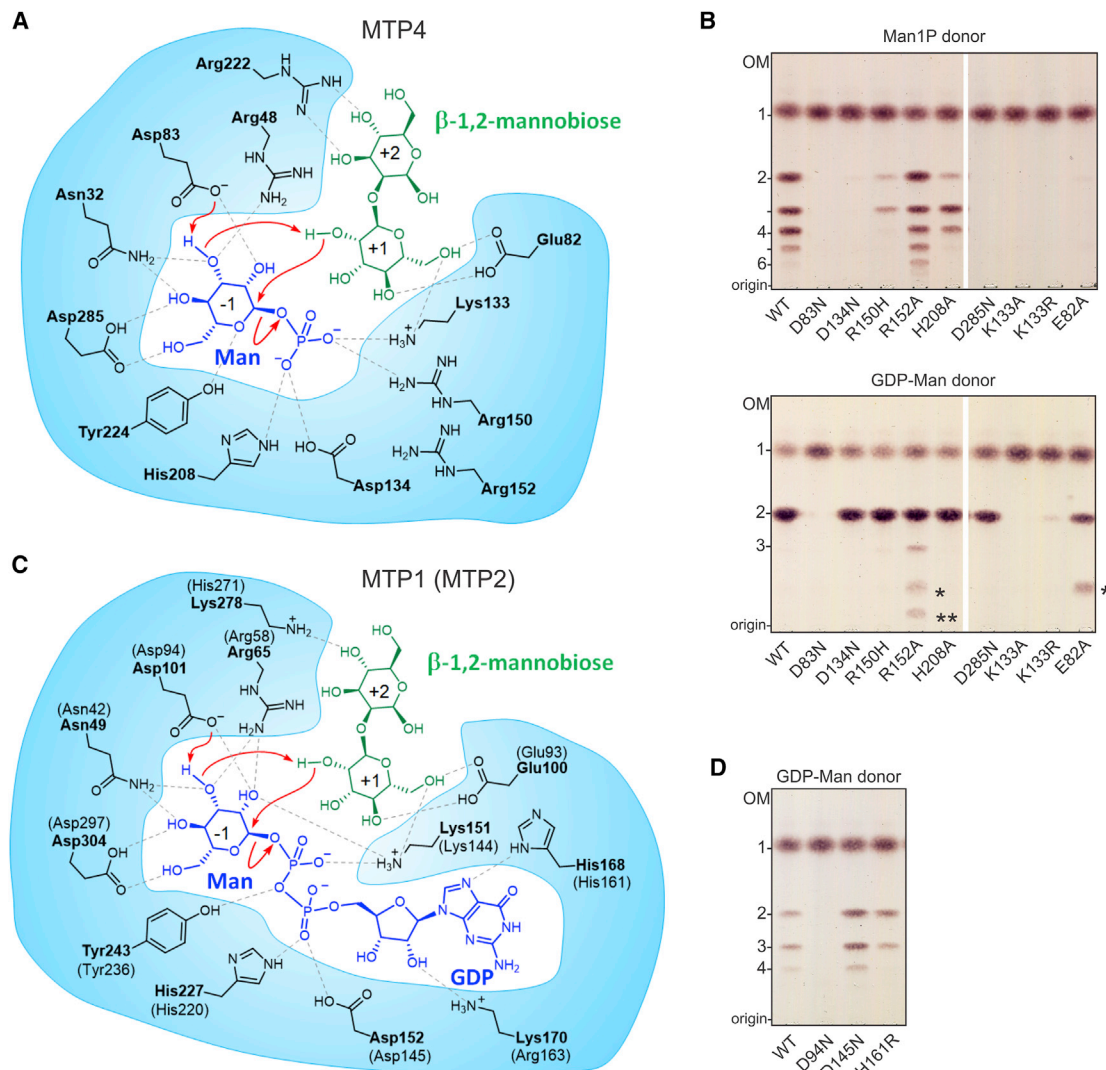See also Figures S2–S6 and Tables S1–S3.

Figure 4. Identification of Key Residues in the *L. mexicana* MTP Catalytic Pocket Required for Phosphorolytic or Mannosyltransferase Activity

(A) 2D interaction map showing hydrogen bonds and electrostatic interactions (black dashed lines) between MTP4 amino acid residues and the Man1P donor and mannogen acceptor combination.

(B) Mutant MTP4 proteins were incubated with OM1 and either Man1P (upper panel) or GDP-Man (lower panel) and the products analyzed by HPTLC.

(C) 2D interaction map of MTP1 active site showing side-chain interactions with GDP-Man and mannogen acceptors. Equivalent MTP2 residues are shown in brackets.

(D) MTP2 mutant proteins were incubated with OM1 and GDP-Man and products analyzed by HPTLC.

See also Figures S3, S5, and S6.

Mannogen levels were elevated in parasite lines lacking the phosphorolytic MTPs, indicating that they are primarily involved in mannogen turnover (Figure 5B). In support of this notion, expression of MTP4 in the *Δmtp3–7* mutant resulted in a modest decrease in mannogen levels (Figure 5B). Complementation of the *L. mexicana Δmtp1–7* null mutant with *MTP3*, *4*, *6*, or *7*, individually or in combination, did not restore mannogen synthesis (Figure S4B), even though the expressed proteins were active in cell lysates (Figure S4C). These data suggest that the phosphorolytic MTPs cannot prime mannogen synthesis *in vivo* either because of limited availability of suitable mannose primers and/or because of

high intracellular Pi levels that drive the reaction in the phosphorolytic direction.

Regulated Mannogen Synthesis Is Required for Infection in the Mammalian Host

Despite growing normally in rich medium at 27°C, *Δmtp1–7* parasites did not induce lesions or proliferate in highly susceptible BALB/c mice (Figures 6A and 6C). Strikingly, expression of MTP1 alone or MTP1/MTP2 together in the absence of phosphorolytic MTPs (*Δmtp1-7::pX-MTP1* and *Δmtp3–7* lines, respectively) exacerbated the loss of virulence phenotype, with no recovery of parasites from tissue biopsies (Figures 6A and 6C).
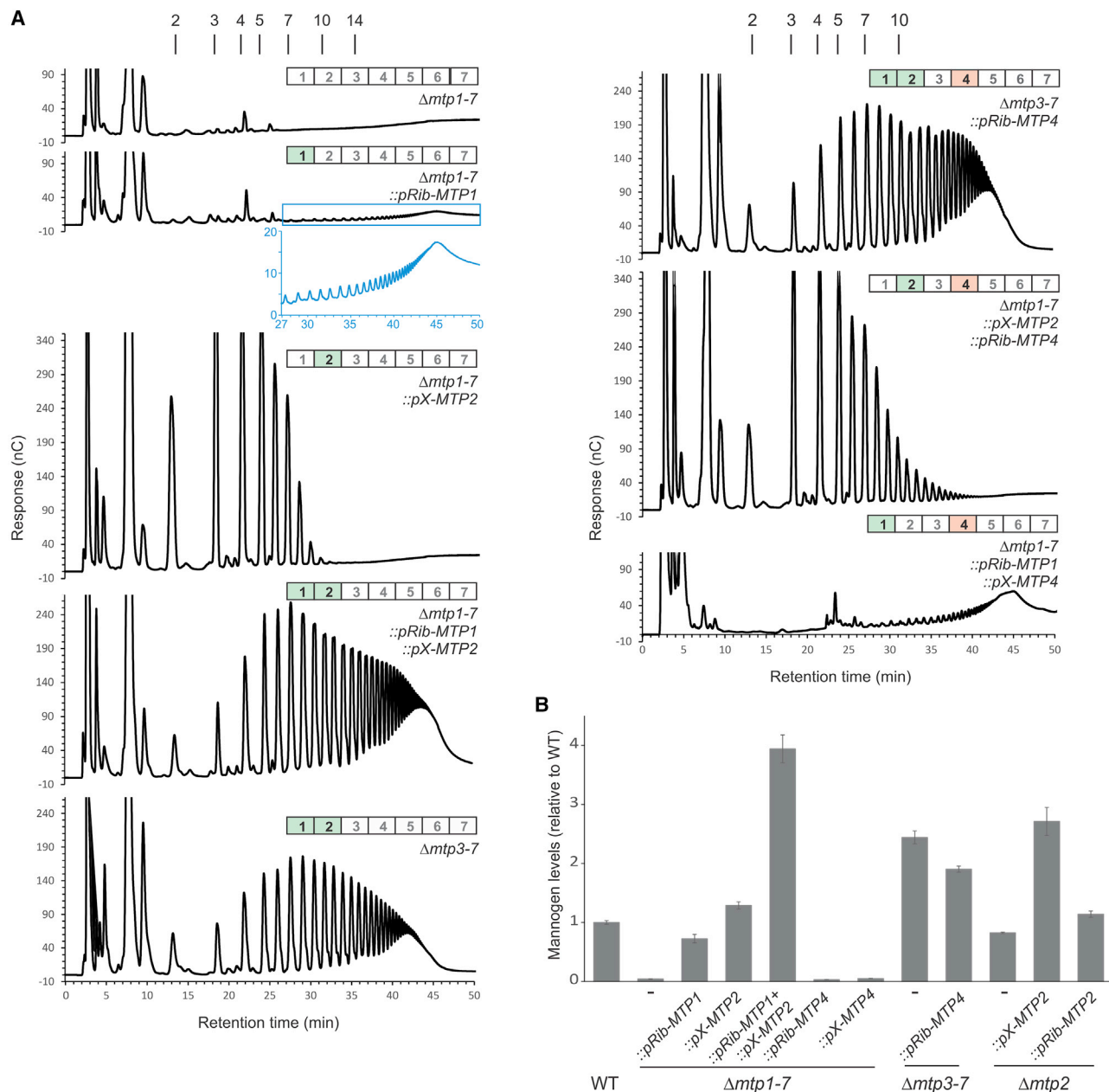
Figure 5. *Leishmania* MTPs Have Non-redundant Functions *In Vivo*

(A) HPAEC-PAD analysis of the mannogen profiles of *L. mexicana Δmtp1–7* and *Δmtp3–7* and complemented lines expressing *MTP* genes on an episomal plasmid (*pX*) or inserted into the ribosomal loci (*pRib*). Expression (green and orange) or absence (no color) of individual *MTP* genes in each line is indicated. The insert shows the hyperextended mannogen chains in *Δmtp1–7::pRib-MTP1* parasites.

(B) Mannogen levels in the different transgenic parasite lines (n = 3 biological replicates). Data presented are mean ± SEM.

See also Figures S4 and S7.

Complementation of *Δmtp1–7* with *MTP2* and *MTP4* also failed to restore virulence (Figure 6A), suggesting that *Leishmania* virulence in animals is highly sensitive to loss of one or more MTPs. As MTP2 plays a key role in regulating mannogen DP *in vivo*, we generated a knockout line lacking only MTP2. The *Δmtp2* mutant did not induce lesions in BALB/c mice even when a high inoculum (10^7 parasites) was used (Figures 6B and S7B). Genetic complementation of this mutant (*Δmtp2::pX-MTP2* or

Δmtp2::pRib-MTP2), restored synthesis of low DP mannogen (Figure S7A) as well as virulence in mice (Figures 6B and S7B), suggesting that mannogen synthesis and/or cycling is critical for survival of mammalian infective stages.

Defects in mannogen synthesis or cycling were also associated with attenuated growth in macrophages (Figure S7C) which, in the case of *Δmtp2*, could be restored by complementation with *MTP2* (Figure S7C). Mannogen synthesis and
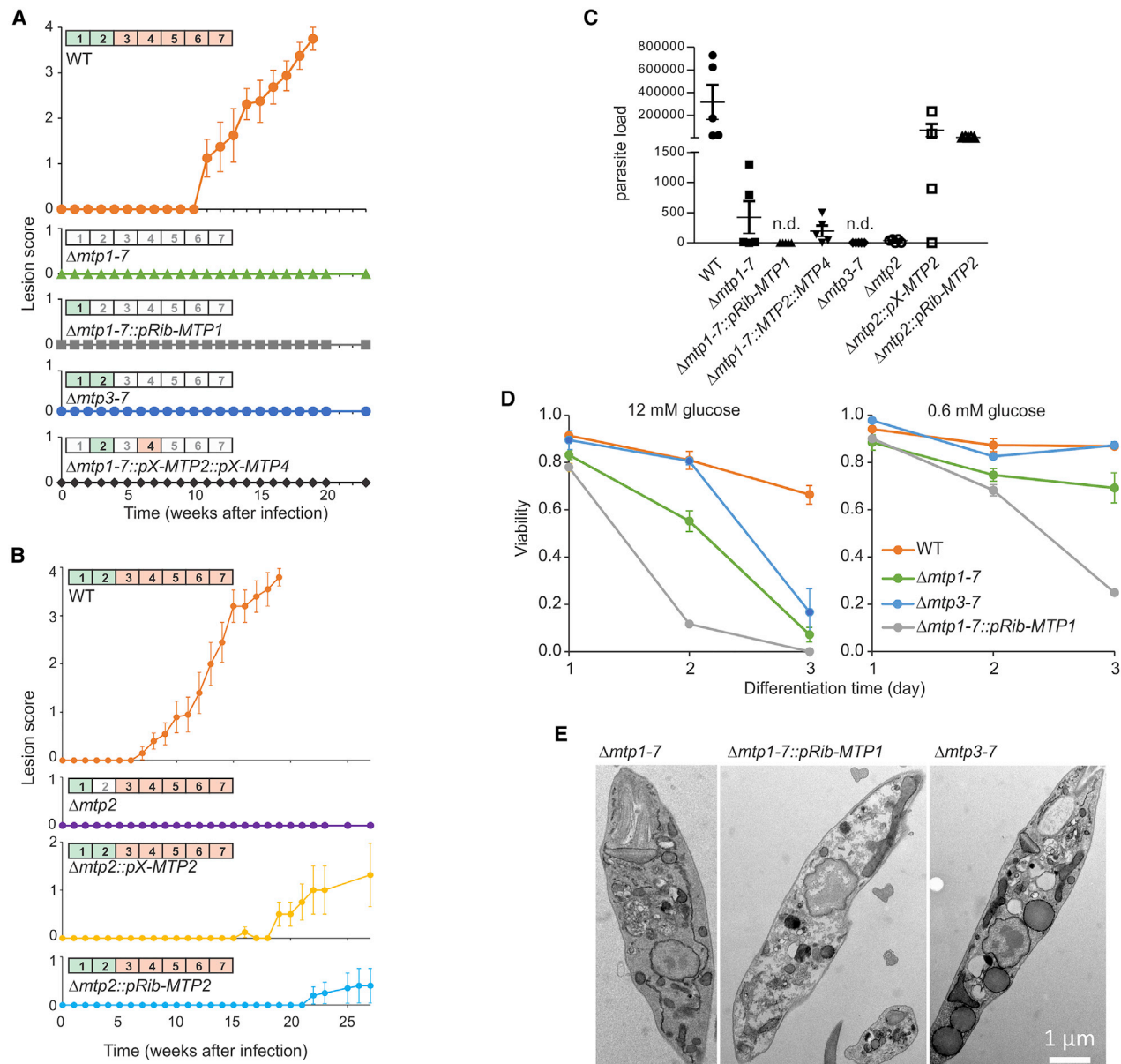
Figure 6. Loss of Single or Multiple *Leishmania* MTPs Leads to Loss of Virulence

(A) Induction of lesions by *L. mexicana* WT, *Δmtp1–7*, *Δmtp3–7* and selected complemented parasite lines in BALB/c mice (n = 5 animals per treatment).

(B) Induction of lesions by *Δmtp2* and corresponding pX- or pRib-*MTP2* complemented lines (n = 5 animals per treatment).

(C) Parasite burden in proximal lymph nodes 23 weeks post infection (n = 5 tissue samples). n.d., no parasites were detected.

(D) WT and *Δmtp* mutant promastigotes were cultivated in medium, pH 5.5, containing either 12 mM or 0.6 mM glucose (33°C for 3 days) and parasite viability determined by propidium iodide staining (n = 3 biological replicates).

(E) TEM ultrastructure of *Δmtp1–7*, *Δmtp1–7::pRib-MTP1* and *Δmtp3–7* promastigotes.

Data presented for (A)–(D) are mean ± SEM.

See also Figure S7.

turnover also appeared to be required for amastigote differentiation as *Δmtp1–7* and *Δmtp3–7* promastigotes lost viability when incubated at elevated temperature (33°C) and low pH (5.5), conditions that normally induce amastigote differentiation (Figures 6D and S7D). Viability was partly rescued if parasites were induced to differentiate in low-glucose medium (Figure 6D), suggesting that mannogen cycling may protect parasites from

glucose toxicity. *Δmtp1–7::pRibMTP1* promastigotes were also acutely sensitive to glucose toxicity (Figure 6D), which likely reflects the hyper-accumulation of high-DP mannogen in these parasites and disruption of the cytoplasm (Figure 6E).

To further assess the role of mannogen synthesis and cycling in regulating glucose homeostasis, *L. mexicana* promastigotes and amastigotes were labeled with $^{13}C_6$-glucose and mannogen
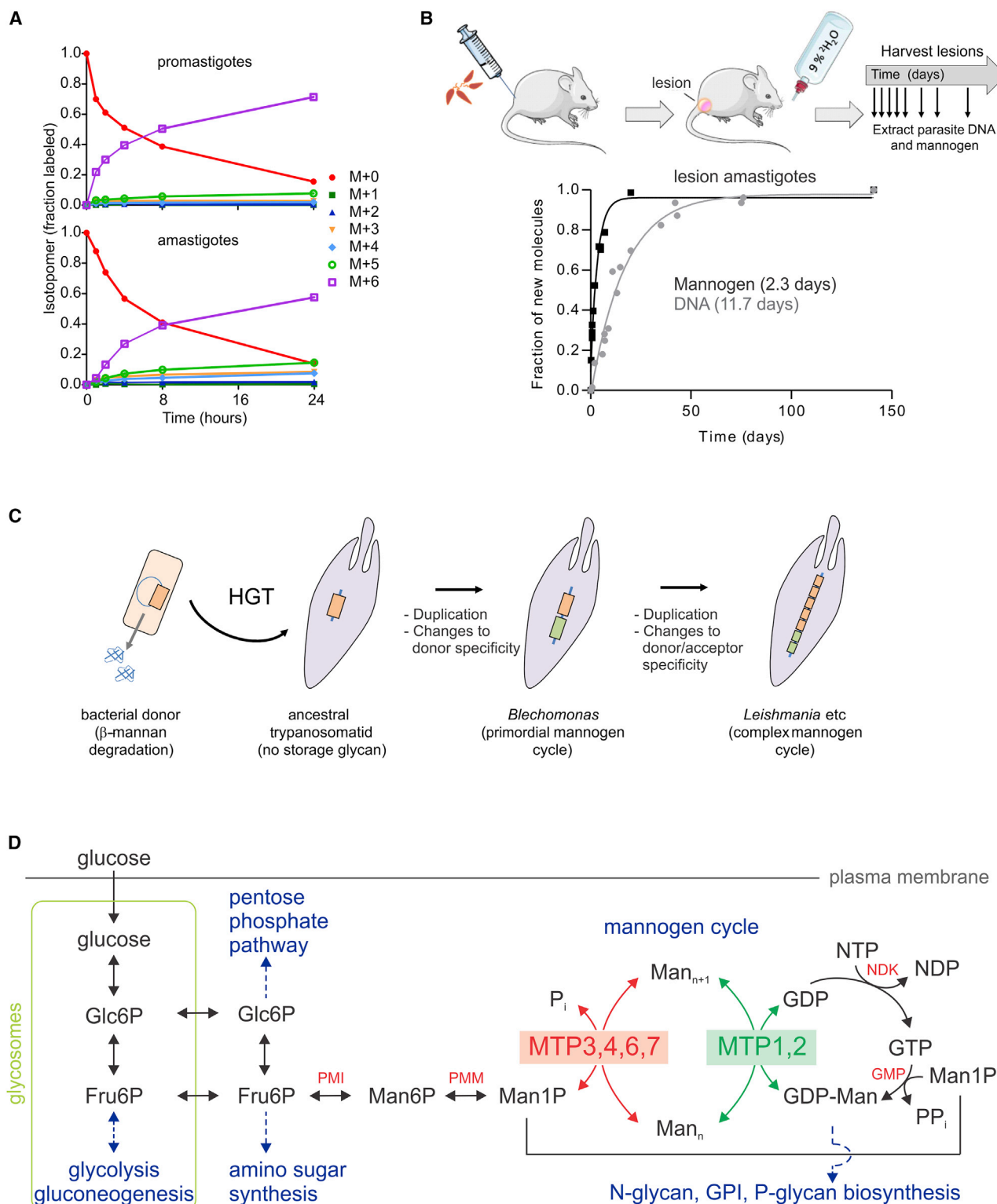
Figure 7. Mannogen is Constitutively Cycled under Nutrient-Replete Growth Conditions *In Vitro* and in Murine Lesions

(A) Incorporation of $^{13}C_6$-glucose into mannogen (M+0 to M+6) in *L. mexicana* promastigotes and axenic amastigotes.

(B) *L. mexicana* infected BALB/c mice were labeled with 9% ^2H_2O and the level of deuterium incorporation into parasite DNA (deoxyribose moiety) and mannogen determined by gas chromatography-mass spectrometry (GC-MS). The $t_{1/2}$ for DNA and mannogen turnover was 11.7 and 2.3 days, respectively.

(C) Proposed evolution of the mannogen cycle in Trypanosomatids by HGT, gene duplication, and changes in MTP donor and/or acceptor specificity.

turnover under glucose-replete conditions measured. Constitutive mannogen turnover was observed in both promastigote ($t_{1/2}$ 4 h) and amastigote stages ($t_{1/2}$ 5 h) (Figure 7A). The high turnover rate of mannogen in amastigotes is notable, as these stages have a 10-fold lower rate of glucose uptake compared to promastigotes (Saunders et al., 2014). Interestingly, most of the mannose in the mannogen pool was fully labeled (M+6), indicating that a significant proportion of exogenous glucose is channeled directly into mannogen synthesis. The accumulation of additional mannose isotopomers (M+3, M+4, and M+5) reflects the recycling of hexose-phosphates (and derived triose-, tetraose-, and pentose-phosphates) through the oxidative and non-oxidative arms of the pentose phosphate pathway (Figure 7A). The complexity of these labeling patterns suggests that mannogen cycling regulates glucose homeostasis and carbon fluxes under glucose-replete conditions.

To investigate whether constitutive mannogen cycling also occurs in metabolically quiescent amastigote stages in tissue granulomas, infected BALB/c mice were labeled with 9% deuterium oxide (^2H_2O) and turnover of parasite DNA and mannogen determined from ^2H-incorporation into the deoxyribose and mannose constituents of these molecules, respectively (Figure 7B). Mannogen turnover was approximately five times faster than DNA ($t_{1/2}$ of 2.3 days versus 11.7 days, respectively) (Kloehn et al., 2015). As mannogen comprises a significant fraction of amastigote biomass (Ralton et al., 2003), mannogen cycling represents a major metabolic flux in these stages.

DISCUSSION

The absence of canonical carbohydrate reserves in all of the Trypanosomatidae suggest that these pathways were lost early in the evolution of the parasitic lifestyles of these protists (Opperdoes et al., 2016). Here, we show that an important subgroup of the Trypanosomatidae, the Leishmaniinae, have subsequently evolved a non-canonical pathway of carbohydrate reserve biosynthesis through the acquisition and functional repurposing of bacterial genes involved in carbohydrate degradation. As a result of gene duplication and donor and/or acceptor diversification, the MTP enzymes catalyze a cycle of mannogen synthesis and turnover that contributes to the regulation of key pathways in central carbon metabolism and is essential for virulence. We propose that the evolution of this pathway has facilitated the colonization of both extracellular and intracellular niches in the insect vectors and mammalian hosts of these parasites.

In most organisms, the biosynthesis and turnover of intracellular carbohydrate reserves is regulated by distinct families of sugar-nucleotide glycosyltransferases and glycan phosphorylases or glycosidases. In contrast, the biosynthesis and cycling of *Leishmania* mannogen is regulated by a single family of glycosyltransferases that contain both GDP-Man-dependent mannosyltransferase and β-1,2-mannogen phosphorylase activities

(Figure 7D). The *Leishmania* MTPs are founding members of the CAZy GT108 family, which includes a large number of bacterial proteins of unknown function. GT108 family members share limited sequence identity but a high degree of structural similarity to the CAZy GH130 family of bacterial β-mannan phosphorylase or mannosidases. The six enzymatically active *Leishmania* MTP proteins share overlapping but non-redundant roles in mannogen biosynthesis and cycling. In particular, MTP1 and MTP2 are responsible for priming mannogen synthesis *in vitro* and *in vivo* and for generating distinct pools of mannogen with high DP (>12) and low DP (2–10), respectively. In contrast, MTP3, 4, 6, and 7 primarily act as phosphorylases *in vitro* and *in vivo* and only exhibit transferase activity on small acceptors (Figure 7D). While these enzymes catalyze the reverse phosphorolytic elongation of mannogen *in vitro*, they cannot prime mannogen synthesis *in vivo* under normal growth conditions. Finally, MTP5 contains key catalytic residues representative of both the transferase and phosphorylase MTPs but lacks detectable enzymatic activity. The function of this protein is unknown.

Phylogenetic analysis showed that the *Leishmania* MTPs are sequence related to a large family of proteins from gram-positive bacteria. Intriguingly, genes encoding proteins in the GT108 family are found in bacteria that are commonly present in the midgut of the modern insect vectors colonized by *Leishmania* and other members of the Leishmaniinae subfamily (Dey et al., 2018). The trypanosomatid *MTP* genes may thus have been acquired by HGT within a similar insect niche, most likely after the split of this group from the trypanosomes (*T. brucei*, *T. cruzi*) (Figure 7C). While the bacterial GT108 genes have yet to be characterized, they contain signature residues of glycan phosphorylases, suggesting a role in the degradation of complex plant glycans in the insect gut or other niches (Nakae et al., 2013). Phylogenetic analysis indicates that acquisition of a GT108 gene in the common Leishmaniinae ancestor was followed by gene duplication and changes in the donor specificity of the primordial MTP proteins. In particular, *B. ayalai*, the most divergent member of the Leishmaniinae, contains three MTP homologs or paralogs, one of which is predicted to be a transferase. The acquisition of MTPs with efficient mannosyltransferase activity is likely to have been the key step in the establishment of a functional mannogen cycle, while the further amplification of this gene family in other members of the Leishmaniinae may have been critical in regulating the overall capacity and flux through this cycle and its responsiveness to different nutrient or growth conditions.

The *Leishmania* MTPs have the same five-bladed β-propeller fold and similar reaction mechanism as bacterial GH130 mannan phosphorylases or hydrolases, although they differ at the sequence level. The MTPs have acquired their dual mannosyltransferase and phosphorylase activities though the acquisition of amino acid changes that expanded the Man1P binding pocket to enhance binding of sugar nucleotides. In particular, the introduction of specific amino acid side chains into the

---

(D) Schematic of the *Leishmania* mannogen cycle. The synthesis of low- and high-DP mannogen is mediated by MTP2 and MTP1, respectively, while turnover is regulated by MTP3, 4, 6, and 7. Constitutive mannogen cycling may regulate intracellular levels of sugar phosphates ATP and Pi/PPi. PMI, phosphomannose isomerase; PMM, phosphomannomutase; GMP, GDP-Man pyrophosphorylase; NDK, nucleotide diphosphate kinase.
See also Figure S7.

phosphate-binding pocket (such as His168/161 in MTP1/MTP2) to bind the guanine moiety demonstrates that GDP is not simply a surrogate for Pi. Interestingly, a number of fungal pathogens, including *Candida albicans*, also synthesize linear β-1,2-mannans, which are incorporated into cell wall and surface glycoconjugates. These glycans are synthesized by family GT91 GDP-Man-dependent β-1,2-mannosyltransferases expressed in the secretory pathway (Sfihi-Loualia et al., 2016). The *C. albicans* mannosyltransferases also share low sequence identity to bacterial GH130 glycan hydrolases and phosphorylases and appear to have independently evolved a similar active site geometry to the *Leishmania* MTPs (Figures S6C and S6E; Table S3). Whether other glycan phosphorylases have also evolved sugar-nucleotide-dependent transferase activities is worthy of further investigation.

Leishmania promastigotes characteristically accumulate high-DP mannogen as they enter stationary phase growth and can rapidly utilize these oligomers under glucose-limiting conditions, suggesting that they primarily function as a canonical energy and carbon reserve in these stages (Ralton et al., 2003). In contrast, the obligate intracellular amastigotes constitutively accumulate high levels (~10 mM) of low-DP mannogen, suggesting a distinct role in mammalian infective stages (Ralton et al., 2003). We have shown that amastigotes enter a slow growing, metabolically quiescent state associated with reduced rates of utilization of glucose and other carbon sources, as well as repression of energy-intensive processes such as transcription and protein translation (Saunders et al., 2014; Kloehn et al., 2015; McConville et al., 2015). In contrast, we show here that low-DP mannogen is constitutively cycled in both cultured and lesion amastigotes. Mannogen cycling may therefore function as a metabolic rheostat, buffering changes in sugar uptake and down-stream fluxes into glycolysis, the pentose phosphate pathway and nucleotide/sugar nucleotide biosynthesis (Figure 7). Mannogen cycling may also have a direct role in modulating intracellular levels of ATP and Pi, which are utilized in the cycle (Figure 7). Importantly, we show that mannogen cycling confers resistance to glucose toxicity and elevated temperatures and is essential for virulence in the mammalian host. *Leishmania* are also exposed to transient and potentially toxic pulses of sucrose (up to 30%) when the sandfly periodically feeds on plant saps and honeydews (Louradour et al., 2017; Dey et al., 2018). Under these conditions, mannogen cycling may prevent catastrophic imbalance in fluxes in upper and lower glycolysis and cell death, as has been proposed for the Pi and nucleotide-triphosphate-consuming trehalose cycle in yeast (van Heerden et al., 2014). The evolution of the mannogen cycle in monogenic trypanosomatid ancestors may thus have allowed these parasites to colonize new insect hosts, as well as to survive and proliferate within the phagolysosomes of macrophages. The central role of mannogen cycling in *Leishmania* central carbon metabolism in the mammalian host suggests that the *Leishmania* MTPs, and in particular MTP2, are potential targets for new therapeutics.

STAR★METHODS

Detailed methods are provided in the online version of this paper and include the following:

- KEY RESOURCES TABLE
- LEAD CONTACT AND MATERIALS AVAILABILITY
- EXPERIMENTAL MODEL AND SUBJECT DETAILS
  - Parasites
  - Bone Marrow Derived Macrophages
  - Mice
  - Bacteria
- METHOD DETAILS
  - Generation of *L. mexicana* Mutants and Complemented Strains
  - Bacterial Gene Expression and Protein Purification
  - GDP-Man-Dependent Mannosyltransferase Assays
  - Mannogen Phosphorylase Assays
  - HPTLC Analysis of Enzyme Products
  - Mannogen Profiling in Wild Type and Mutant Parasite Lines
  - GC-MS and LC-MS Analysis of Unlabeled and ^{13}C-/^{2}H-Labeled Mannogen
  - Chemical and Enzymatic Analyses
  - Macrophage Infection
  - Mouse Infections
  - Microscopy
  - Protein Production for Crystallization and SECMALS
  - Crystallization of MTP1, MTP2 and MTP4
  - X-ray Data Collection and Crystal Structure Solution
  - SECMALS
  - Phylogenetic Analysis
  - Homology Modeling and Molecular Docking
  - Multiple Sequence Alignments and Phylogenetic Tree Building for the GT108 MTPs, and GH130 Proteins
- QUANTIFICATION AND STATISTICAL ANALYSIS
- DATA AND CODE AVAILABILITY

DECLARATION OF INTERESTS

The authors declare no competing interests.

REFERENCES

Agirre, J., Iglesias-Fernández, J., Rovira, C., Davies, G.J., Wilson, K.S., and Cowtan, K.D. (2015). Privateer: software for the conformational validation of carbohydrate structures. Nat. Struct. Mol. Biol. *22*, 833–834.

Bañuls, A.L., Bastien, P., Pomares, C., Arevalo, J., Fisa, R., and Hide, M. (2011). Clinical pleiomorphism in human leishmaniases, with special mention of asymptomatic infection. Clin. Microbiol. Infect. *17*, 1451–1461.

Benzel, I., Weise, F., and Wiese, M. (2000). Deletion of the gene for the membrane-bound acid phosphatase of *Leishmania mexicana*. Mol. Biochem. Parasitol. *111*, 77–86.

Burza, S., Croft, S.L., and Boelaert, M. (2018). Leishmaniasis. Lancet *392*, 951–970.

Chambers, M.C., Maclean, B., Burke, R., Amodei, D., Ruderman, D.L., Neumann, S., Gatto, L., Fischer, B., Pratt, B., Egertson, J., et al. (2012). A cross-platform toolkit for mass spectrometry and proteomics. Nat. Biotechnol. *30*, 918–920.

Cobbold, S.A., Chua, H.H., Nijagal, B., Creek, D.J., Ralph, S.A., and McConville, M.J. (2016). Metabolic dysregulation induced in *Plasmodium falciparum* by dihydroartemisinin and other front-line antimalarial Drugs. J. Infect. Dis. *213*, 276–286.

Crooks, G.E., Hon, G., Chandonia, J.-M., and Brenner, S.E. (2004). WebLogo: a sequence logo generator. Genome Res. *14*, 1188–1190.

Cuskin, F., Baslé, A., Ladevèze, S., Day, A.M., Gilbert, H.J., Davies, G.J., Potocki-Véronèse, G., and Lowe, E.C. (2015). The GH130 Family of Mannoside Phosphorylases Contains Glycoside Hydrolases That Targetβ-1,2-Mannosidic Linkages in Candida Mannan. J. Biol. Chem. *290*, 25023–25033.

Dereeper, A., Guignon, V., Blanc, G., Audic, S., Buffet, S., Chevenet, F., Dufayard, J.-F., Guindon, S., Lefort, V., Lescot, M., et al. (2008). Phylogeny.fr: robust phylogenetic analysis for the non-specialist. Nucleic Acids Res. *36*, W465–W469.

Dey, R., Joshi, A.B., Oliveira, F., Pereira, L., Guimarães-Costa, A.B., Serafim, T.D., de Castro, W., Coutinho-Abreu, I.V., Bhattacharya, P., Townsend, S., et al. (2018). Gut microbes egested during bites of infected sand flies augment severity of leishmaniasis via inflammasome-Derived IL-1β. Cell Host Microbe *23*, 134–143.

Edgar, R.C. (2004). MUSCLE: multiple sequence alignment with high accuracy and high throughput. Nucleic Acids Res. *32*, 1792–1797.

Emsley, P., Lohkamp, B., Scott, W.G., and Cowtan, K. (2010). Features and development of Coot. Acta Crystallogr. D Biol. Crystallogr. *66*, 486–501.

François, J., and Parrou, J.L. (2001). Reserve carbohydrates metabolism in the yeast *Saccharomyces cerevisiae*. FEMS Microbiol. Rev. *25*, 125–145.

Garami, A., and Ilg, T. (2001). Disruption of mannose activation in *Leishmania mexicana*: GDP-mannose pyrophosphorylase is required for virulence, but not for viability. EMBO J. *20*, 3657–3666.

Guindon, S., Dufayard, J.-F., Lefort, V., Anisimova, M., Hordijk, W., and Gascuel, O. (2010). New algorithms and methods to estimate maximum-likelihood phylogenies: assessing the performance of PhyML 3.0. Syst. Biol. *59*, 307–321.

Ha, D.S., Schwarz, J.K., Turco, S.J., and Beverley, S.M. (1996). Use of the green fluorescent protein as a marker in transfected *Leishmania*. Mol. Biochem. Parasitol. *77*, 57–64.

Hanssen, E., Dekiwadia, C., Riglar, D.T., Rug, M., Lemgruber, L., Cowman, A.F., Cyrklaff, M., Kudryashev, M., Frischknecht, F., Baum, J., and Ralph, S.A. (2013). Electron tomography of *Plasmodium falciparum* merozoites re-veals core cellular events that underpin erythrocyte invasion. Cell. Microbiol. *15*, 1457–1472.

He, Z., Zhang, H., Gao, S., Lercher, M.J., Chen, W.H., and Hu, S. (2016). Evolview v2: an online visualization and management tool for customized and annotated phylogenetic trees. Nucleic Acids Res. *44* (W1), W236–W241.

Huerta-Cepas, J., Serra, F., and Bork, P. (2016). ETE 3: Reconstruction, Analysis, and Visualization of Phylogenomic Data. Mol. Biol. Evol. *33*, 1635–1638.

Jackson, A.P., Otto, T.D., Aslett, M., Armstrong, S.D., Bringaud, F., Schlacht, A., Hartley, C., Sanders, M., Wastling, J.M., Dacks, J.B., et al. (2016). Kinetoplastid Phylogenomics Reveals the Evolutionary Innovations Associated with the Origins of Parasitism. Curr. Biol. *26*, 161–172.

Jubb, H.C., Higueruelo, A.P., Ochoa-Montaño, B., Pitt, W.R., Ascher, D.B., and Blundell, T.L. (2017). Arpeggio: A Web Server for Calculating and Visualising Interatomic Interactions in Protein Structures. J. Mol. Biol. *429*, 365–371.

Katoh, K., and Standley, D.M. (2013). MAFFT multiple sequence alignment software version 7: improvements in performance and usability. Mol. Biol. Evol. *30*, 772–780.

Keegan, F.P., and Blum, J.J. (1992). Utilization of a carbohydrate reserve comprised primarily of mannose by *Leishmania donovani*. Mol. Biochem. Parasitol. *53*, 193–200.

Kitaoka, M. (2015). Diversity of phosphorylases in glycoside hydrolase families. Appl. Microbiol. Biotechnol. *99*, 8377–8390.

Kloehn, J., Saunders, E.C., O'Callaghan, S., Dagley, M.J., and McConville, M.J. (2015). Characterization of metabolically quiescent *Leishmania parasites* in murine lesions using heavy water labeling. PLoS Pathog. *11*, e1004683.

Konagurthu, A.S., Whisstock, J.C., Stuckey, P.J., and Lesk, A.M. (2006). MUSTANG: a multiple structural alignment algorithm. Proteins *64*, 559–574.

Laskowski, R.A., Rullmann, J.A., MacArthur, M.W., Kaptein, R., and Thornton, J.M. (1996). AQUA and PROCHECK-NMR: programs for checking the quality of protein structures solved by NMR. J. Biomol. NMR *8*, 477–486.

LeBowitz, J.H., Coburn, C.M., McMahon-Pratt, D., and Beverley, S.M. (1990). Development of a stable *Leishmania* expression vector and application to the study of parasite surface antigen genes. Proc. Natl. Acad. Sci. USA *87*, 9736–9740.

Lombard, V., Golaconda Ramulu, H., Drula, E., Coutinho, P.M., and Henrissat, B. (2014). The carbohydrate-active enzymes database (CAZy) in 2013. Nucleic Acids Res. *42*, D490–D495.

Louradour, I., Monteiro, C.C., Inbar, E., Ghosh, K., Merkhofer, R., Lawyer, P., Paun, A., Smelkinson, M., Secundino, N., Lewis, M., et al. (2017). The midgut microbiota plays an essential role in sand fly vector competence for *Leishmania major*. Cell. Microbiol. *19*, e12755.

MacNeill, G.J., Mehrpouyan, S., Minow, M.A.A., Patterson, J.A., Tetlow, I.J., and Emes, M.J. (2017). Starch as a source, starch as a sink: the bifunctional role of starch in carbon allocation. J. Exp. Bot. *68*, 4433–4453.

McConville, M.J., Homans, S.W., Thomas-Oates, J.E., Dell, A., and Bacic, A. (1990). Structures of the glycoinositolphospholipids from *Leishmania major*. A family of novel galactofuranose-containing glycolipids. J. Biol. Chem. *265*, 7385–7394.

McConville, M.J., Saunders, E.C., Kloehn, J., and Dagley, M.J. (2015). *Leishmania* carbon metabolism in the macrophage phagolysosome- feast or famine? F1000Res. *4* (F1000 Faculty Rev), 938.

McCoy, A.J., Grosse-Kunstleve, R.W., Adams, P.D., Winn, M.D., Storoni, L.C., and Read, R.J. (2007). Phaser crystallographic software. J. Appl. Cryst. *40*, 658–674.

McNicholas, S., Potterton, E., Wilson, K.S., and Noble, M.E. (2011). Presenting your structures: the CCP4mg molecular-graphics software. Acta Crystallogr. D Biol. Crystallogr. *67*, 386–394.

Melamud, E., Vastag, L., and Rabinowitz, J.D. (2010). Metabolomic analysis and visualization engine for LC-MS data. Anal. Chem. *82*, 9818–9826.

Misslitz, A., Mottram, J.C., Overath, P., and Aebischer, T. (2000). Targeted integration into a rRNA locus results in uniform and high level expression of

transgenes in *Leishmania* amastigotes. Mol. Biochem. Parasitol. *107*, 251–261.

Murshudov, G.N., Skubák, P., Lebedev, A.A., Pannu, N.S., Steiner, R.A., Nicholls, R.A., Winn, M.D., Long, F., and Vagin, A.A. (2011). REFMAC5 for the refinement of macromolecular crystal structures. Acta Crystallogr. D Biol. Crystallogr. *67*, 355–367.

Naderer, T., Wee, E., and McConville, M.J. (2008). Role of hexosamine biosynthesis in *Leishmania* growth and virulence. Mol. Microbiol. *69*, 858–869.

Naderer, T., Heng, J., and McConville, M.J. (2010). Evidence that intracellular stages of *Leishmania major* utilize amino sugars as a major carbon source. PLoS Pathog. *6*, e1001245.

Nakae, S., Ito, S., Higa, M., Senoura, T., Wasaki, J., Hijikata, A., Shionyu, M., Ito, S., and Shirai, T. (2013). Structure of novel enzyme in mannan biodegradation process 4-O-β-D-mannosyl-D-glucose phosphorylase MGP. J. Mol. Biol. *425*, 4468–4478.

Oliveira, D.M., Costa, M.A.F., Chavez-Fumagalli, M.A., Valadares, D.G., Duarte, M.C., Costa, L.E., Martins, V.T., Gomes, R.F., Melo, M.N., Soto, M., et al. (2012). Evaluation of parasitological and immunological parameters of *Leishmania chagasi* infection in BALB/c mice using different doses and routes of inoculation of parasites. Parasitol. Res. *110*, 1277–1285.

Opperdoes, F.R., Butenko, A., Flegontov, P., Yurchenko, V., and Lukeš, J. (2016). Comparative metabolism of free-living *Bodo saltans* and parasitic trypanosomatids. J. Eukaryot. Microbiol. *63*, 657–678.

Peng, J., and Xu, J. (2011). RaptorX: exploiting structure information for protein alignment by statistical inference. Proteins *79* (*Suppl 10*), 161–171.

Potterton, L., Agirre, J., Ballard, C., Cowtan, K., Dodson, E., Evans, P.R., Jenkins, H.T., Keegan, R., Krissinel, E., Stevenson, K., et al. (2018). CCP4i2: the new graphical user interface to the CCP4 program suite. Acta Crystallogr. D Struct. Biol. *74*, 68–84.

Previato, J.O., Xavier, M.T., Brazil, R.P., Gorin, P.A., and Mendonça-Previato, L. (1984). Formation of (1——2)-linked beta-D-mannopyranan by Leishmania mexicana amazonensis: relationship with certain Crithidia and Herpetomonas species. J. Parasitol. *70*, 449–450.

Ralton, J.E., Naderer, T., Piraino, H.L., Bashtannyk, T.A., Callaghan, J.M., and McConville, M.J. (2003). Evidence that intracellular beta1-2 mannan is a virulence factor in Leishmania parasites. J. Biol. Chem. *278*, 40757–40763.

Robert, X., and Gouet, P. (2014). Deciphering key features in protein structures with the new ENDscript server. Nucleic Acids Res. *42*, W320–W324.

Saburi, W. (2016). Functions, structures, and applications of cellobiose 2-epimerase and glycoside hydrolase family 130 mannoside phosphorylases. Biosci. Biotechnol. Biochem. *80*, 1294–1305.

Sali, A., Potterton, L., Yuan, F., van Vlijmen, H., and Karplus, M. (1995). Evaluation of comparative protein modeling by MODELLER. Proteins *23*, 318–326.

Saunders, E.C., Ng, W.W., Kloehn, J., Chambers, J.M., Ng, M., and McConville, M.J. (2014). Induction of a stringent metabolic response in intracellular stages of *Leishmania mexicana* leads to increased dependence on mitochondrial metabolism. PLoS Pathog. *10*, e1003888.

Senoura, T., Ito, S., Taguchi, H., Higa, M., Hamada, S., Matsui, H., Ozawa, T., Jin, S., Watanabe, J., Wasaki, J., and Ito, S. (2011). New microbial mannan catabolic pathway that involves a novel mannosylglucose phosphorylase. Biochem. Biophys. Res. Commun. *408*, 701–706.

Sernee, M.F., Ralton, J.E., Dinev, Z., Khairallah, G.N., O'Hair, R.A., Williams, S.J., and McConville, M.J. (2006). *Leishmania* beta-1,2-mannan is assembled on a mannose-cyclic phosphate primer. Proc. Natl. Acad. Sci. USA *103*, 9458–9463.

Sfihi-Loualia, G., Hurtaux, T., Fabre, E., Fradin, C., Mée, A., Pourcelot, M., Maes, E., Bouckaert, J., Mallet, J.-M., Poulain, D., et al. (2016). *Candida albicans* β-1,2-mannosyltransferase Bmt3 prompts the elongation of the cell-wall phosphopeptidomannan. Glycobiology *26*, 203–214.

Shi, L., Sutter, B.M., Ye, X., and Tu, B.P. (2010). Trehalose is a key determinant of the quiescent metabolic state that fuels cell cycle progression upon return to growth. Mol. Biol. Cell *21*, 1982–1990.

Simonetti, F.L., Teppa, E., Chernomoretz, A., Nielsen, M., and Marino Buslje, C. (2013). MISTIC: Mutual information server to infer coevolution. Nucleic Acids Res. *41*, W8–W14.

Singh, O.P., Hasker, E., Sacks, D., Boelaert, M., and Sundar, S. (2014). Asymptomatic *Leishmania* infection: a new challenge for *Leishmania* control. Clin. Infect. Dis. *58*, 1424–1429.

Stein, N. (2008). CHAINSAW: a program for mutating pdb files used as templates in molecular replacement. J. Appl. Cryst. *41*, 641–643.

Stuart, K., Brun, R., Croft, S., Fairlamb, A., Gürtler, R.E., McKerrow, J., Reed, S., and Tarleton, R. (2008). Kinetoplastids: related protozoan pathogens, different diseases. J. Clin. Invest. *118*, 1301–1310.

Tsuda, T., Nihira, T., Chiku, K., Suzuki, E., Arakawa, T., Nishimoto, M., Kitaoka, M., Nakai, H., and Fushinobu, S. (2015). Characterization and crystal structure determination of β-1,2-mannobiose phosphorylase from *Listeria innocua*. FEBS Lett. *589* (24 Pt B), 3816–3821.

van der Peet, P., Gannon, C.T., Walker, I., Dinev, Z., Angelin, M., Tam, S., Ralton, J.E., McConville, M.J., and Williams, S.J. (2006). Use of click chemistry to define the substrate specificity of Leishmania beta-1,2-mannosyltransferases. ChemBioChem *7*, 1384–1391.

van der Peet, P., Ralton, J.E., McConville, M.J., and Williams, S.J. (2012). Discovery of inhibitors of *Leishmania* β-1,2-mannosyltransferases using a click-chemistry-derived guanosine monophosphate library. PLoS One *7*, e32642.

van Heerden, J.H., Wortel, M.T., Bruggeman, F.J., Heijnen, J.J., Bollen, Y.J.M., Planqué, R., Hulshof, J., O'Toole, T.G., Wahl, S.A., and Teusink, B. (2014). Lost in transition: start-up of glycolysis yields subpopulations of nongrowing cells. Science *343*, 1245114.

Winter, G. (2010). xia2: an expert system for macromolecular crystallography data reduction. J. Appl. Cryst. *43*, 186–190.

Winter, G., Lobley, C.M.C., and Prince, S.M. (2013). Decision making in xia2. Acta Crystallogr. D Biol. Crystallogr. *69*, 1260–1273.

Ye, Y., Saburi, W., Odaka, R., Kato, K., Sakurai, N., Komoda, K., Nishimoto, M., Kitaoka, M., Mori, H., and Yao, M. (2016). Structural insights into the difference in substrate recognition of two mannoside phosphorylases from two GH130 subfamilies. FEBS Lett. *590*, 828–837.

Zimmermann, L., Stephens, A., Nam, S.-Z., Rau, D., Kübler, J., Lozajic, M., Gabler, F., Söding, J., Lupas, A.N., and Alva, V. (2018). A completely reimplemented MPI bioinformatics Toolkit with a new HHpred server at its core. J. Mol. Biol. *430*, 2237–2243.

STAR★METHODS

KEY RESOURCES TABLE

REAGENT or RESOURCE	SOURCE	IDENTIFIER
Bacterial and Virus Strains		
XL10-Gold	Agilent	Cat#210515
XL-1-Blue	Agilent	Cat#200249
BL21(DE3)pLysS	Agilent	Cat#200132
Biological Samples		
Canavalia ensiformis (jack bean) α-mannosidase	Sigma	Cat#M7257
Helix pomatia (snail) β-mannosidase	Sigma	Cat#M9400
Chemicals, Peptides, and Recombinant Proteins		
OM1	Williams laboratory	van der Peet et al., 2012
OM4	This study	N/A
GDP-[2-^{3}H]-Man	McConville laboratory	N/A
GDP-Man (guanosine 5′-diphospho-D-mannose sodium salt)	Sigma	Cat#G5131-50 mg
GDP (Guanosine 5′-diphosphate sodium salt)	Sigma	Cat#G7127-100 mg
α-Man1P	Sapphire Bioscience	Cat#M185010
β-Man1P	Williams laboratory	N/A
D-Glucose-U-^{13}C	Sigma	Cat#297046
^{2}H$_2$O	Cambridge isotope laboratories	Cat#DLM-4-99-1000
Critical Commercial Assays		
PiColorLock Gold phosphate assay	Innova Biosciences	Cat#303-0030
Deposited Data		
L. mexicana LmxM.10.1230 no ligand (MTP1)	This study	PDB: 6Q4W
L. mexicana LmxM.10.1240 no ligand (MTP2)	This study	PDB: 6Q4X
L. mexicana LmxM.10.1240 + Man (MTP2 + Man)	This study	PDB: 6Q4Y
L. mexicana LmxM.10.1240 D94N + β-1,2-mannobiose (MTP2 D94N + β-1,2-mannobiose)	This study	PDB: 6Q4Z
L. mexicana LmxM.10.1260 + Pi (MTP4 + Pi)	This study	PDB: 6Q50
Experimental Models: Cell Lines		
Δgmp	T. Ilg	Garami and Ilg, 2001
Δpmi	T. Ilg	Garami and Ilg, 2001
Δpmm	T. Ilg	Garami and Ilg, 2001
Δmtp1-7	This study	N/A
Δmtp3-7	This study	N/A
Δmtp2	This study	N/A
pRib-MTP1	This study	N/A
Δmtp1-7::pRib-MTP1	This study	N/A
Δmtp1-7::pRib-MTP2	This study	N/A
Δmtp1-7::pX-MTP2	This study	N/A
Δmtp1-7::pRib-MTP-1/pX-MTP2	This study	N/A
Δmtp1-7::pRib-MTP1/pX-MTP4	This study	N/A

(Continued on next page)

Continued

REAGENT or RESOURCE	SOURCE	IDENTIFIER
Δ*mtp1-7::pRib-MTP4*	This study	N/A
Δ*mtp1-7::pX-MTP4*	This study	N/A
Δmtp1-7::pX-MTP2 + pRib-MTP4	This study	N/A
Δ*mtp1-7::pX-MTP3+4*	This study	N/A
Δ*mtp-1-7::pX-MTP3+4/ pRib-MTP5+6*	This study	N/A
Δ*mtp-1-7::pX-MTP4+7*	This study	N/A
Δ*mtp1-7::pX-MTP4+7/ pRib-MTP5+6*	This study	N/A
Δ*mtp3-7::pRib-MTP4*	This study	N/A
Δ*mtp3-7::pX-MTP2/ pRib-MTP4*	This study	N/A
Δ*mtp2::pX-MTP2*	This study	N/A
Δ*mtp2::pRib-MTP2*	This study	N/A
Experimental Models: Organisms/Strains		
L. mexicana (MNYC/ BZ/ 62/M379)	ATCC	Cat#50156
BALB/c mice	Animal Resources Centre, Canning Vale, WA, Australia	Cat#BC
Oligonucleotides		
Primers for MTP knockout constructs and confirmation, see Table S4	This study	N/A
Primers for MTP expression, see Table S4	This study	N/A
Primers for deletion mutants, see Table S4	This study	N/A
Recombinant DNA		
pET-28a(+)	Novagen	Cat#69864-3
pGEX-6p-3	GE Healthcare	Cat#28-9546-51
pGEX-4T-2	GE Healthcare	Cat#28-9545-50
pRIBII	JC Mottram laboratory	Misslitz et al., 2000
pX-Neo	SM Beverley laboratory	LeBowitz et al., 1990
pX-Hyg	This study	N/A
pBluescript II SK+	Statagene	GenBank Acc#X52328
pXG-BLEO (PHLEO)	SM Beverley laboratory http://beverleylab.wustl.edu/plasmids_vectors.html	B3324
pXG-SAT	SM Beverley laboratory http://beverleylab.wustl.edu/plasmids_vectors.html	B2352
pXG-'GFP+	SM Beverley laboratory http://beverleylab.wustl.edu/plasmids_vectors.html	B2863
Knockout constructs (pBluescript-SKII(+)) made, Table S5	This study	N/A
Expression (including deletion) constructs (pGEX-4T-2, pGEX-6p-3 and pET28a(+)), Table S5	This study	N/A
Software and Algorithms		
Prism 5	GraphPad	https://www.graphpad.com/
AXIOVISION 4.8	Zeiss	N/A
Modeler v9.20	Sali et al., 1995	https://salilab.org/modeller/9.20/release.html
SYBYL-X 2.1.1	Certara	https://www.certara.com/
PROCHECK	Laskowski et al., 1996	https://www.ebi.ac.uk/thornton-srv/software/PROCHECK/
PyMOL Molecular graphics system, version 1.8.2.2	Schrodinger	https://pymol.org/2/
MUSTANG v3.2.3	Konagurthu et al., 2006	http://lcb.infotech.monash.edu.au/mustang/

REAGENT or RESOURCE	SOURCE	IDENTIFIER
ETE3 v3.1.1	Huerta-Cepas et al., 2016	http://etetoolkit.org/
PhyML v3.12	Guindon et al., 2010	http://www.atgc-montpellier.fr/phyml/versions.php/
TreeDyn v198.3	Dereeper et al., 2008	http://www.phylogeny.fr/one_task.cgi?task_type=treedyn
ESPript3.0	Robert and Gouet, 2014	http://espript.ibcp.fr/ESPript/ESPript/index.php
ClustalW	N/A	http://www.mybiosoftware.com/bioedit-7-0-9-biological-sequence-alignment-editor.html
ClustalΩ	Zimmermann et al., 2018	https://toolkit.tuebingen.mpg.de/
RaptorX	Peng and Xu, 2011	http://raptorX.uchicago.edu/StructurePrediction/predict/
MAFFT v7.0	Katoh and Standley, 2013	https://mafft.cbrc.jp/alignment/server/
Evolview	He et al., 2016	https://www.evolgenius.info//evolview/
MISTIC	Simonetti et al., 2013	N/A
Arpeggio	Jubb et al., 2017	http://biosig.unimelb.edu.au/arpeggioweb/
WebLogo 3	Crooks et al., 2004	N/A
DIALS		https://dials.diamond.ac.uk/
Xia2	Winter et al., 2013	https://xia2.github.io/
Aimless	Potterton et al., 2018	http://www.ccp4.ac.uk/html/aimless.html
Phaser	McCoy et al., 2007	https://www.phaser.cimr.cam.ac.ukindex.php/Phaser_Crystallographic_Software; http://www.ccp4.ac.uk/
CCP4mg	McNicholas et al., 2011	http://www.ccp4.ac.uk/MG/
Chainsaw	Stein, 2008	http://www.ccp4.ac.uk/html/chainsaw.html
Refmac5	Murshudov et al., 2011	https://www2.mrc-lmb.cam.ac.uk/groups/murshudov/content/refmac/refmac.html
Coot	Emsley et al., 2010	https://www2.mrc-lmb.cam.ac.uk/personal/pemsley/coot/
Ccp4i2 GUI	Potterton et al., 2018	https://www.ccp4.ac.uk/ccp4i_main.php
Privateer	Agirre et al., 2015	http://www.ccp4.ac.uk/html/privateer.html
ASTRA software		https://www.wyatt.com/products/software/astra.html
MSD-ChemStation	Agilent Technologies	N/A
MassHunter	Agilent Technologies	N/A
MS convert	Chambers et al., 2012	http://proteowizard.sourceforge.net/tools.shtml
Maven	Melamud et al., 2010	http://genomics-pubs.princeton.edu/mzroll/index.php

LEAD CONTACT AND MATERIALS AVAILABILITY

Further information requests for resources and reagents should be directed to and will be fulfilled by the Lead Contact, Malcolm J. McConville (malcolmm@unimelb.edu.au).

EXPERIMENTAL MODEL AND SUBJECT DETAILS

Parasites

L. mexicana (MNYC/BZ/62/M379) promastigotes were grown in Roswell Park Memorial Institute (RPMI)-1640 medium (Invitrogen) containing 10% heat inactivated fetal bovine serum (FBS, Invitrogen), pH 7.4 at 27°C. Mutant and complemented parasite lines were cultivated in the presence of appropriate antibiotics: Geneticin (100 μg/mL, GIBCO), Puromycin (20 μg/mL, Sigma), Hygromycin

B (50 μg/mL, InvivoGen), Bleomycin (10 μg/mL, Calbiochem), Nourseothricin (100 μg/mL, JenaBioscience). Stationary phase pro-promastigotes were induced to differentiate to amastigotes by cultivation in RPMI, 20% FBS, pH 5.5 at 33°C (Saunders et al., 2014). For ^{13}C-glucose labeling experiments, *L. mexicana* promastigotes or amastigotes were suspended in RPMI-1640 medium containing ^{13}C-U-glucose (6 mM) and harvested with rapid chilling to quench metabolism at indicated time points (Saunders et al., 2014). For ^{3}H-mannose labeling experiments, *L. mexicana* wild type promastigotes (3 × 10^8) were pulse labeled in glucose-free RPMI-1%BSA medium containing D-[2-^{3}H]-mannose (50μCi/mL) for 5 min, harvested by rapid centrifugation (1,000 *x g*, 30 s) and washed in ice cold phosphate buffered saline (x 3), prior to hypotonic lysis.

Bone Marrow Derived Macrophages
Bone marrow macrophages (BMDM) were isolated from BALB/c mice. Cells were flushed from tibia of hind-legs of mice seeded in TC Petri dishes at 1x10^7 cells/plate in 10 mL RPMI containing 15% FBS, 20% L929-cell medium (containing macrophage colony stimulating factor; MCSF) and incubated at 37°C, 5% CO$_2$. After 24 h non-adherent progenitor cells from each dish were transferred to two non-TC Petri dishes. Progenitor cells converted to macrophages within 3-4 days. At day 3 after differentiation, 1 mL extra L929-cell medium was added to the plate. At day 5, cells were removed from the plates and plated onto coverslips in 24 well plates at 1x10^5 cells/well in RPMI containing 15% FBS, 10% L929-cell medium.

Mice
Mice usage was approved by the Institutional Animal Care and Use Committee of the University of Melbourne (ethics number 1212647.1). All animal experiments were performed in accordance with the Australian National Health Medical Research Council (NHMRC) (Australian code of practice for the care and use of animals for scientific purposes, 8th edition, 2013, ISBN: 1864965975). Mice used in this study were maintained in the biological research facility of the Bio21 Molecular Science and Biotechnology Institute under specific pathogen free (SPF) conditions according to institutional guidelines. BALB/c mice were gender (female) and age matched (6-8 weeks) within individual experiments. Mice were bred in house or purchased from Animal Resources Centre, Canning Vale, WA, Australia (product code: BC; SPF status in health report). Animals were not subject to water or food restrictions and monitored daily by facility staff.

Bacteria
The strain and source of all the bacteria used in this study are detailed in Key Resources Table.

METHOD DETAILS

Generation of *L. mexicana* Mutants and Complemented Strains
The *L. mexicana* Δ*mtp1-7* null mutant was generated by homologous replacement of the entire LmxM.10.1230-LmxM.10.1290 gene locus with bleomycin and nourseothricin resistant cassettes. The bleomycin and nourseothricin resistance cassettes were digested from pXG-BLEO and pXG-SAT, respectively, using the EcoRI and BamHI restriction sites, and cloned into the pBluescript II SK+ vector. The 745 bp 5′UTR region of LmxM.10.1230 was amplified using forward and reverse primers (Table S4) and cloned into pBluescriptII SK+ vector already containing the resistance cassettes using the *Hind*III and *Bst*BI restriction sites. The 952 bp 3′UTR region of LmxM.10.1290 was cloned into these plasmids after amplification and digest using the BamHI and *Xba*I restriction sites. The resulting bleomycin and nourseothricin knock-out constructs were verified by sequencing. *L. mexicana* was transfected with 2-5 μg *Hind*III and *Xba*I digested and gel-purified linearized DNA fragments. Drug resistant clones were screened by PCR for the presence of the resistance cassettes using a forward primer in the 5′UTR outside the cloned region and a reverse primer for the resistance bleomycin and nourseothricin cassettes and the absence of the genes using 5′and 3′primers of each gene (Table S4).

The *L. mexicana* Δ*mtp3-7* null mutant was generated using the above constructs, but with the 5′UTR region of LmxM.10.1230 replaced with the 5′UTR 896 bp region of LmxM.10.1250 amplified from wild type cDNA using forward and reverse primers (Table S4) and was cloned using the *Hind*III and *Bst*BI restriction sites. *L. mexicana* was transfected as described below and null mutants were screened as described above, with its specific primers (Table S4)

The *L. mexicana* Δ*mtp2* null mutant was generated by sequential deletion of both LmxM.10.1240 genes using a linearized constructs of plasmids that were constructed as follows: The 740 bp 5′ UTR region of LmxM.10.1240 was amplified using primers indicated in Table S4 and cloned using HindIII and BstBI restriction sites into a pBluescript II SK+ vector already containing the either a bleomycin or nourseothricin resistance gene and the 896 bp 3′ UTR region of LmxM.10.1240 was amplified using primers indicated in Table S4 and cloned using BamHI and XbaI restriction sites. Positive clones were verified as described above (specific primers indicated in Table S4)

Complementation of the Δ*mtp1-7, Δmtp3-7 and Δmtp2* mutants was achieved by expression of individual genes from the pXG episome or by stable insertion into the ribosomal RNA loci as described below (Misslitz et al., 2000; Benzel et al., 2000). LmxM.10.1260 was expressed in the Δ*mtp1-7* mutant as a C-terminal GFP fusion protein using pXG-'GFP+ (B2863) (Ha et al., 1996), using the primers from Table S4 with the XmaI and *Eco*RV restriction sites. For stable integration into the ribosomal RNA locus, LxmM.10.1260 and LmxM.10.1230 genes were amplified using *Blg*II and *Not*I containing primers and both were cloned into the pRIBII plasmid using *Blg*II and *Not*I restriction sites (Benzel et al., 2000; Misslitz et al., 2000).

LmxM.10.1240 was expressed using an episomal expression construct without tag under the selection of hygromycin. LmxM.10.1240 was amplified using primers from Table S4 and cloned using *Bam*HI and *Not*I restriction sites in pX-Hyg derived from pX-Neo vector by replacing the neo/DHFR between *Spe*I sites of pX with the hygromycin gene using splice overlap PCR. LmxM.10.1270 and LmxM.10.1280 were amplified with the intergenic region and cloned in pRIBII plasmid (Benzel et al., 2000; Misslitz et al., 2000) for stable integration into the ribosomal RNA locus for constitutive expression. The LxmM.10.1270-80 region was amplified with the forward primers of LmxM.10.1270 and reverse primer of LmxM.10.1280 (see Table S4).

pX-Hyg constructs with LmxM.10.1250 and LmxM10.1290 were made by inserting BglII and *Not*I amplified material in *Bam*HI and *Not*I digested plasmid using primers listed in Table S4.

For transfection, promastigotes (mid-log phase, 4×10^7 cells/transfection) were suspended in chilled electroporation buffer (EPB; 21 mM HEPES, 137 mM NaCl, 5 mM KCl, 6 mM glucose, 0.7 mM Na_2PO_4 pH 7.4), in a 4 mm cuvette and electroporated with 3-5 μg of linearized DNA or 5-10 μg of circular (uncut) plasmid DNA and pulsed twice at 1,700 V and 25 μF with a 10 s interval in a BioRad Gene Pulser. Cells were transferred to SDM-79 media containing 10% FBS and 100 units/mL penicillin/streptomycin. After 24 h the medium was supplemented with selection drugs.

Bacterial Gene Expression and Protein Purification

L. mexicana MTPs were expressed in *E. coli* using pGEX-6p-3, pGEX-4T-2 or pET-28a(+) plasmids resulting in N-terminal GST-tag for pGEX or His-tag for pET plasmid (Table S5). The *MTP* encoding gene was amplified from cDNA with either a BglII or *Bam*HI restriction site and *Not*I and was cloned into pGEX vectors using *Bam*HI and *Not*I sites or into pET-28a(+) using *Nde*I and *Not*I restriction sites. *MTP* constructs in the pGEX-6p-3 expression vector were used as templates for mutagenesis. Mutations were introduced with QuickChange Lightning Multi Site-Directed Mutagenesis Kit (Agilent Technologies) according to the manufacturer's instructions. Once sequences were confirmed, the DNA was subsequently amplified with primers containing *Nde*I and *Not*I restriction sites for cloning into pET-28(a)+.

Recombinant proteins were expressed in BL21(DE3)-pLysS at 37°C at 220 rpm until OD_{600} reached approximately 0.8 (Table S5). The culture was allowed to adapt to 16°C for 2 h (240 rpm), before being induced with 0.1 mM IPTG for > 16 h at 16°C at 240 rpm. Protein was extracted from cell pellets in 4 mL Bugbuster (Merck Millipore) containing protease inhibitors without EDTA (Roche) per 50 mL culture pellet for 10 min.

GST-tagged protein was purified from 25,000 x g supernatants using Glutathione Sepharose 4B (GE-healthcare) washed with 10 volumes of PBS before being eluted with 10 mM glutathione in 50 mM Tris pH 8.0. His-tagged protein was purified from 25,000 x g supernatants using Complete His-Tag Purification resin (Roche) (1 ml) equilibrated with 5 mM imidazole, 500 mM NaCl, 20 mM Tris-HCl, pH 7.9. The resin was washed with increased imidazole concentrations from 5, 20, 45 to 60 mM in 500 mM NaCl, 20 mM Tris-HCl, pH 7.9 and protein was eluted with 250 mM imidazole in 500 mM NaCl, 20 mM Tris-HCl, pH 7.9. Amicon Ultra-15 (10K) centrifugal filters (Merck Millipore) were used to exchange buffers to low ionic strength assay buffer (5 mM NaHEPES-NaOH buffer, pH 7.4 with 5 mM $MgCl_2$, 1 mM $MnCl_2$, 2 mM EGTA and 2 mM DTT) or with 20 mM MES, 2 mM EGTA, pH 5.5.

GDP-Man-Dependent Mannosyltransferase Assays

Mannosyltransferase activities in parasite lysates or of recombinant proteins were measured using octyl-α-mannosides (OM1) or octyl-mannogen (DP 4 (OM4), or DP 1-16 (OM1-16)) as acceptors and either unlabeled GDP-Man or GDP-[2-^{3}H]-Man as donors. The use of OM_n acceptors facilitated the recovery of products by solvent phase partitioning and analysis by HPTLC and were used with similar affinity as corresponding native mannogen oligomers. In brief, cell lysates were prepared by hypotonic lysis of *L. mexicana* wild type or *Δgmp* promastigotes harvested at late log growth phase (van der Peet et al., 2012). Promastigotes (4 x10^7 /assay) were washed in cold PBS then suspended in 50 μl of cold hypotonic lysis buffer (1 mM HEPES-NaOH buffer, pH 7.4, containing 2 mM EGTA, 2 mM DTT and protease inhibitors without EDTA (Roche)) and incubated for 10 min on ice. Cell lysis was monitored by microscopy and facilitated by brief bath sonication (3-5 s) if required. Lysed cells were centrifuged (2000 *x g*, 4°C, 4 min) and the supernatant removed. The pellet was washed with 10 vol of low ionic strength assay buffer (5 mM NaHEPES-NaOH buffer, pH 7.4 with 2 mM EGTA, 2 mM DTT and protease inhibitors without EDTA (Roche)). The supernatant was adjusted to 5 mM HEPES buffer, pH 7.4 with 2 mM EGTA, 2 mM DTT and protease inhibitors without EDTA (Roche) and the pellet fractions suspended in the same buffer containing 0.1% TX-100, to achieve the same cell equivalents. Assays were initiated by addition of acceptor (native mannogen or OM1), and GDP-[2-^{3}H]-Man (50 μM) /unlabeled GDP-Man (0.05-10 mM), and incubated at 27°C for indicated times. Reactions were stopped by addition of chloroform/methanol (1:2 v/v) to give a final ratio of chloroform/ methanol/ aqueous 1:2:0.8 (v/v), centrifuged (15,000 rpm, 5 min), and the supernatant dried under nitrogen. OM_n products were recovered by phase partitioning between water-saturated 1-butanol (200 μl) and water (150 μl), the 1-butanol phase dried and analyzed by high performance TLC (HPTLC). For analysis of longer OM products, extracts were desalted by passage down a small column (400 μl) of Ag 50-X12(H$^+$) over Ag 4-X4(OH$^-$) (Bio-Rad) and freeze-dried prior to HPTLC analysis. For assay of recombinant proteins, final reaction mixtures contained 50 μl of 20 mM MES-NaOH, pH 5.5, 5-10 μg purified recombinant protein, 0.05-5 mM OM1, OM4 or OM1-16 as acceptor, and 0.05-10 mM GDP-Man or GDP as donor. Reactions were initiated by addition of protein and reactions (27°C, 5-90 min) stopped and processed as described above. OM4 was generated by incubating *L. mexicana* MTP2 with OM1 (5 mM) and GDP-Man (10 mM) at 27°C for 90 min, and purified by preparative HPTLC on Silica Gel 60 coated aluminum backed HPTLC sheets (Merck), developed

twice in 1-butanol: ethanol: water (4:3:3 v/v). Silica bands containing individual octyl-mannogen species were scraped from the HPTLC plates and extracted in water-saturated 1-butanol (2 × 200 μl).

Mannogen Phosphorylase Assays

L. mexicana promastigote lysates prepared from wild type or the *Δpmm* mutant line (lacking the enzyme phosphomannosemutase) as described above were incubated with ^{3}H-mannogen. Hypotonic lysates were adjusted to contain 5 mM HEPES buffer, pH 7.4, protease inhibitors without EDTA (Roche), EDTA, and 10^6 cell equivalents/mL. ^{3}H-mannogen was prepared by metabolically labeling stationary phase promastigotes of *L. mexicana Δpmi* in glucose-free RPMI-1%BSA medium containing D-[2-^{3}H]-mannose for 4 h at 27°C (Sernee et al., 2006). The absence of phosphomannose isomerase in this mutant line maximizes efficiency of labeling. Labeled parasites were extracted in hot water (100°C, 10 min) and mannogen oligomers desalted over a small ion exchange column of AG 50W-X12(H$^+$) over AG 4-X4(OH$^-$) (Bio-Rad) (100 μl each) and freeze-dried. Phosphorylase assays were initiated by incubating 100 μl lysate and ^{3}H-mannogen (10,000 dpm) at 27°C for 2 h. Assays were stopped by addition of chloroform/methanol (1:2 v/v) as described above and neutral and phosphorylated sugar products analyzed by HPAEC. For analysis of recombinant MTP proteins, assays contained 50 μl 20 mM MES-NaOH, pH 5.5, 5-10 μg recombinant protein and either NaHPO$_4$ (0.5-5 mM) or Man1P (1 mM) in the case of reverse phosphorolysis, and OM4 (200 μM mannose equivalent) or unlabeled mannogen (2 mM mannose equivalent) as substrate. After incubation at 27°C for 90 min, reactions were stopped by heating at 100°C for 2 min and either the C8Man$_x$ products were analyzed by HPTLC after desalting as described above, or release of phosphate was measured using the PiColorLock Gold phosphate assay (Innova Biosciences).

HPTLC Analysis of Enzyme Products

Desalted reaction products were analyzed by HPTLC on Silica Gel 60 aluminum-backed HPTLC sheets (Merck), developed twice in 1-butanol: ethanol: water (4:3:3 v/v) for neutral glycans or polar samples, or once in chloroform: methanol: 13 M ammonia: 1 M ammonium acetate: water (180:140:9:9:23 v/v) for apolar samples (Ralton et al., 2003). Unlabeled glycans were visualized by staining with 0.2% orcinol (Sigma-Aldrich) in 10% H$_2$SO$_4$, 80% ethanol and developed at 100°C. Labeled species were detected by fluorography after spraying the HPTLC sheets with EN^{3}HANCE spray (PerkinElmer Life Sciences) and exposing them to Biomax MR film (Kodak) at −80°C.

Mannogen Profiling in Wild Type and Mutant Parasite Lines

Parasites were metabolically quenched by transferring aliquots of culture suspension into 15 mL plastic tube and immersion into a dry ice-ethanol bath for 20 s (until suspension reached 5°C). The chilled suspension (8 × 10^7 parasites) was centrifuged (4,000 rpm, 0°C, 10 min), washed three times with ice-cold PBS, then suspended in 200 μl ice-cold water and immersed in a boiling water bath for 20 min. The extracts were centrifuged (16,000 x g, 15 min) and the supernatant containing mannogen desalted over a small ion exchange column of AG 50W-X12(H$^+$) over AG 4-X4(OH$^-$) (Bio-Rad). In some cases, extracts were hydrolyzed in 80 mM TFA (100°C, 10 min) to cleave acid labile phosphate mono-esters, prior to desalting. Sugar-phosphates, neutral sugars and mannogen oligosaccharides were analyzed by HPAEC, using a Dionex GP-50 gradient pump, a CarboPac PA-1 column (4 × 250 mm), with a PA-1 guard column and an ED$_{50}$ integrated pulsed amperometric detector (PAD). The system was controlled and data analyzed by Chromeleon version 6.50 software. Sugar phosphates were resolved on a gradient of 1 mM sodium hydroxide (E1) and 1 mM sodium hydroxide containing 1 M sodium acetate (E2) at a flow rate of 1 mL/min: $T_0 = 98\%$ (v/v) E1; $T_{15} = 98\%$ (v/v) E1; $T_{30} = 90\%$ (v/v) E1; $T_{40} = 80\%$ (v/v) E1; $T_{55} = 100\%$ (v/v) E2; $T_{65} = 100\%$ (v/v) E2. Neutral sugars/oligosaccharides were resolved on a gradient of 75 mM NaOH (E1) and 75 mM NaOH containing 250 mM sodium acetate (E2) at a flow rate of 0.6 mL/min: $T_0 = 100\%$ (v/v) E1; $T_5 = 100\%$ (v/v) E1; $T_{40} = 100\%$ (v/v) E2, $T_{60} = 100\%$ (v/v) E2.

GC-MS and LC-MS Analysis of Unlabeled and ^{13}C-/^{2}H-Labeled Mannogen

Mannogen was extracted from promastigotes in hot water as described above, desalted and resuspended in 20% 1-propanol. For analysis of mannose isotopomers in the mannogen pool, an aliquot of the mannogen extract was subjected to solvolysis in 0.5 M methanolic HCl (50 μl, Supelco) in sealed glass capillaries under vacuum or in deactivated GC-MS glass vial inserts (Agilent part no: 5181-8872) (80°C, 16 h). Samples were neutralized by addition of pyridine (10 μl), dried under nitrogen, and derivitized with N,O-Bis (trimethylsilyl) trifluoroacetamide containing 1% TMCS (40 μl; Thermo Scientific) prior to being analyzed on either an Agilent 6890/5973 GC-MS system in electron impact mode or an Agilent 7890/5975 system in chemical ionization mode. Separation was achieved on a 30 m DB-5ms GC capillary column (J&W scientific; 250 μm i.d., 0.25 μm film thickness), incorporating a 10 m inert duraguard section. The levels of mannogen-derived mannose were quantified by GC-MS in EI mode by determining the total area under the curve for its specific peak (an authentic standard was used to confirm the retention time and ion fragmentation of mannose following methanolysis and silylation). Equal cell equivalents (1x10^7 cells) were analyzed for each genotype and the mannose levels were normalized to an internal standard added during the hot water extraction. Selected ion monitoring was used to quantify the labeling in mannose and its mass isotopologs (M$_0$-M$_6$; 467-473 m/z; a fragment of the mannose derivative associated with loss of CH$_4$ [M+1-16]$^+$). The ^{2}H-labeling in mannogen-derived mannose was determined as the excess molar enrichment in the M$_1$ mass isotopolog (468 m/z) over the molecular ion M$_0$ (467 m/z). GC-MS data was analyzed using MSD ChemStation and MassHunter (Agilent technologies). For LC-MS analysis detection of GDP and GDP-Man, reaction mixtures were separated on a Merck ZIC-pHILIC column (5 μM, 150 × 4.6 mm, Millipore) (Cobbold et al., 2016). A gradient of water with 20 mM ammonium carbonate (solvent A) and

acetonitrile (solvent B) ran from 80%–20% solvent B from 0.5 to 15 min, then 20%–5% between 15 and 20 min, before returning to 80% at 20.5 min and held until 29.5 min. MS detection was performed on an Agilent QTOF mass spectrometer 6545 operating in negative ESI mode and data analyzed using the MAVEN software package (Melamud et al., 2010). Following alignment, metabolites were assigned using exact mass (< 10 ppm) and retention time (compared to standards of GDP and GDP-Man). The area top for each positively assigned metabolite was integrated and the concentration of each metabolite in each sample was determined from standard curves that were acquired for both GDP and GDP-Man.

Chemical and Enzymatic Analyses

Glycan products of recombinant enzyme reactions as well as native mannogen were desalted and subjected to methylation linkage analysis as previously described (McConville et al., 1990). Neutral glycans were digested with *Canavalia ensiformis* (jack bean) α-mannosidase or *Helix pomatia* (snail) β-mannosidase (both Sigma-Aldrich) in 0.1 M sodium acetate, pH 5.0 (2 Units/20 μl) or in 0.1 M citric acid phosphate buffer, pH 4.5 (0.5 Units/20 μl), respectively. Reactions were stopped by incubation at 100°C for 2 min, then desalted over a small column of AG 50W-X12(H$^+$) over AG 4-X4(OH$^-$) (Bio-Rad) (as described above) prior to HPTLC analysis.

Macrophage Infection

BALB/c bone marrow derived macrophages were seeded on 10 mm glass coverslips (1 × 10^5 macrophages/well in 24-well plates) and incubated in RPMI containing 15% FBS and 10% L929-cell conditioned medium at 33°C, 5% CO$_2$ for 24 h prior to infection with *L. mexicana* wild type and mutant promastigotes (1x10^6 cells/well) to give a final MOI of 1:10. Non-internalized parasites were removed after 4 h by washing the monolayer three times with PBS, and infected macrophages incubated as described above. Coverslips were washed with PBS (x3) at different time points after infection, fixed in 4% paraformaldehyde in PBS and stained with Hoechst 33342 (20 μg/mL, Molecular Probes). Slides were mounted in MoWiol and images acquired using a Zeiss Axioplan2 imaging microscope, equipped with AxioCam MRm camera and the AXIOVISION 4.8 software (Zeiss) (Naderer et al., 2010)

Mouse Infections

BALB/c mice (female, 6-8 weeks old) were injected subcutaneously in the hind-rump and lesion size scored weekly as previously described (Naderer et al., 2008). Parasite burden was also monitored at time of death by removal of the right draining inguinal lymph-nodes and limiting dilution cloning of homogenized tissues (Oliveira et al., 2012). For *in vivo* labeling studies, infected mice were injected intra-peritoneal with ^{2}H$_2$O (99%, 35 μl/g body weight), then provided with 9% ^{2}H$_2$O in the drinking water to maintain a level of labeling of 5% in the body (Kloehn et al., 2015). Levels of ^{2}H$_2$O in the body water was regularly checked by GC-MS analysis of blood samples (Kloehn et al., 2015). Mice were culled at indicated time after initiation of labeling and lesion amastigotes isolated from granulomatous lesions as previously described (Kloehn et al., 2015). Purified parasites were washed three times with ice cold PBS, then extracted in hot water (100°C, 20 min). Extracted mannogen was desalted on a small ion exchange column and ^{2}H-labeling in incorporated mannose residues measured by GC-MS.

Microscopy

For fluorescence microscopy, live *Leishmania* promastigotes were incubated with propidium iodide (final 20 μg/mL) for 5 min before being immobilized on L-lysine (Sigma) coated coverslips. Images were acquired by using a Zeiss Axioplan2 imaging microscope, equipped with AxioCam MRm camera and the AXIOVISION 4.8 software (Zeiss). For transmission microscopy, parasites were fixed in 0.1 M sodium cacodylate containing 2.5% glutaraldehyde overnight at 4°C and further processed using the ROTO technique (Hanssen et al., 2013). Sections (70 nm) were visualized on a Tecnai F30 (FEI, Eindhoven) and images captured on a Ceta CMOS 4k x 4k camera (FEI, Eindhoven).

Protein Production for Crystallization and SECMALS

Genes encoding N-terminally His-tagged variants of MTP1, 2, and 4 were expressed in *E. coli* BL21 (DE3) cells. An overnight starter culture was used to inoculate (at 1% v/v) liter-scale TB expression media containing 35 mg/l of kanamycin. The cultures were shaken in 2 L plastic flasks at 37°C at 220 rpm until the OD$_{600}$ was above 1.5. Gene expression was induced by adding a sterile-filtered solution of IPTG to the culture up to a concentration of 1 mM. The temperature was subsequently reduced to 16°C and the cultures were shaken overnight at 220 rpm. The cells were harvested by centrifugation at > 5000 x *g* for 20 min, after which a pellet was formed. The pellet was stored at −80°C until further use. Pellet thawing was done by adding 10 x w/v of 50 mM sodium phosphate pH 6.2, 200 mM NaCl, 1 mM DTT, 30 mM imidazole buffer and gently mixing at RT until fully thawed. Subsequently, the volume was adjusted to 100 mL with the same buffer and the cells were lysed by sonication. The resulting solution was centrifuged at > 30,000 x *g* for 30 min; only the supernatant was collected for further use and loaded onto a 5 mL nickel affinity column (HisTrap FF (GE)). After washing with the abovementioned buffer, the protein was eluted in an imidazole gradient (up to 400 mM). Any precipitated protein was removed by centrifugation and the solution was concentrated to 1-2 ml. The concentrated sample was loaded onto a size-exclusion column (Superdex S75 or S200 (GE)) pre-equilibrated in 50 mM sodium phosphate pH 6.2, 200 mM NaCl, 1 mM DTT buffer. Protein-bearing fractions were collected and the protein was concentrated up to 12 mg/mL (MTP1), 60 mg/mL (MTP2) and 18 mg/mL (MTP4).

Crystallization of MTP1, MTP2 and MTP4

All proteins were crystallized using either sitting drop or hanging drop methods. In the former, the droplet sits on a plastic plate surface and the plates sealed using adhesive film. In the latter, the droplet hangs above the reservoir solution on a siliconized coverslip and the well is sealed with vacuum grease. MTP1 crystals were obtained in 12% w/v PEG 20K, 100 mM MES pH 6.5. The droplet contained 50 nL crystal seed stock solution obtained from previous experiments, 250 nL 5.5 mg/mL protein solution and 200 nL reservoir solution. MTP2 and MTP2 D94N variant crystals were obtained in either 200 mM trisodium citrate, 18%–22% w/v PEG 3350 or in 200 mM triammonium citrate pH 7.0, 18%–22% PEG 3350. The droplet contained a 1:1 ratio of protein (12 mg/mL) to reservoir solution (a total volume of 1 μl for sitting drop and 2 μl for hanging drop). MTP4 was crystallized in 100 mM PCTP pH 7.0, 25% w/v PEG 1500. The droplet contained 150 nL 7 mg/mL protein solution and 150 nL reservoir solution.

X-ray Data Collection and Crystal Structure Solution

Diffraction data were collected at Diamond Light Source synchrotron at beamlines I03, I04 and I24. Crystallographic data were indexed and integrated using Diamond Light Source autoprocessing pipelines that incorporate DIALS software into Xia2 (Winter, 2010). Data truncation, merging and scaling was performed in Aimless. The structures of MTP2 and 4 were solved using molecular replacement (MR) in Phaser (McCoy et al., 2007) with the initial model being 2B4W (PDB code) truncated in Chainsaw (Stein, 2008). The structure of MTP1 was solved using MR in Phaser as well, and the starting model was the polypeptide chain of MTP2. Subsequently, the structures were refined in Refmac5 (Murshudov et al., 2011) and real-space refinement was done using Coot (Emsley et al., 2010). In case of isomorphous crystals in complex with different ligands, the HKL index of the complex was matched to the first obtained solution, the R_{free} set was copied and a model containing the protein only was directly refined to the observed data using Refmac5. Waters were added after the refinement of the polypeptide chain was complete and the ligand molecules were added in the last steps of the refinement. The model geometry and the correspondence of the model to experimental data were validated using Coot validation tools and the PDB validation pipeline. Sugar geometry was validated using Privateer. The process of model building, refinement and validation was performed using the CCP4i2 GUI (Potterton et al., 2018). Data and refinement statistics are shown in Table S1.

SECMALS

Size Exclusion Chromatography Multiangle Light Scattering (SECMALS) was used to investigate the protein assembly molecular weight in solution. The pump used was a Shimadzu HPLC system (CBM-20A Controller, LC-20AD Pump with degasser, SIL-20A Autosampler and SPD-20A detector) and Wyatt detectors: HELEOS-II (light scattering) and Optilab rEx (refractive index). The proteins were kept in 50 mM sodium phosphate pH 6.2, 200 mM NaCl, 1 mM DTT buffer at 3 mg/mL. A standard solution of bovine serum albumin (BSA) was used to calibrate the instrument, as its exact molecular weight and amount used was known. The flow through a Superdex S75 column was kept at a constant 0.5 mL/min. Data were analyzed using ASTRA software (Wyatt Technology).

Phylogenetic Analysis

Sequences of the seven MTP proteins were queried against the NCBI non-redundant sequence database (NR) and TritrypDB release 40 using *blastp* and hits filtered based on e-value (< $1e^{-50}$). Multiple sequence alignments for 21 NR and 148 TritrypDB sequences were generated using MAFFT v7.310 (Katoh and Standley, 2013). Phylogenetic trees were generated based on the multiple sequence alignments with PhyML, with initial tree generation done with BIONJ and the LG substitution model employed with branch support with bootstrap analyses (100). Tree diagrams were generated with Evolview (He et al., 2016) and annotated based on taxonomy mapped using the ETE3 Toolkit (Huerta-Cepas et al., 2016).

Co-evolution analysis was performed using the MISTIC platform (Simonetti et al., 2013), which uses Mutual Information (MI) to infer coevolution between residue pairs, using a MI Z-score threshold of > 6.5, leading to a specificity of 95%. Residue pairings with strong coevolution signals were assessed, and their interactions analyzed using Arpeggio (Jubb et al., 2017). Sequence conservation of protein active site and co-evolving residues was visualized using WebLogo 3 (Crooks et al., 2004).

Homology Modeling and Molecular Docking

Models for *L. mexicana* MTP3, MTP5, MTP6 and MTP7 were constructed using the crystal structure of *L. mexicana* MTP4 as the template. The amino acid sequence identity of these MTPs with *L. mexicana* MTP4 is: MTP3 = 57%, MTP5 = 53%, MTP6 = 60% and MTP7 = 68% (ClustalW as implemented in BioEdit v7.2.5). The four *L. mexicana* MTP homology models were generated using Modeler v9.20 (Sali et al., 1995). Steric clashes between amino acid side chains that may have arisen during model construction were removed by replacing the clashing side chains with an alternative low energy side chain conformation from a conformer library within the Biopolymer module of the modeling program SYBYL-X 2.1.1 (Certara; https://www.certara.com/). Each model was then geometry optimized for 1000 iterations (or until the gradient of successive iterations was < 0.05 kcal/mol · Å) using the molecular mechanics MMFF94s force field and partial atomic charges and conjugate gradient minimization method (all other parameters were at default values) within SYBYL-X 2.1.1. The resulting four *L. mexicana* MTP models were deemed to be good quality models using PROCHECK, with > 99.6% of residues in the allowed regions of the Ramachandran plot (Laskowski et al., 1996).

The amino acid sequence identity between the seven *L. mexicana* MTPs and GH130 family members is very low (5%–12%, ClustalW). To compare the 3-D structures, the four *L. mexicana* MTP models, along with the crystal structures of *L. mexicana* MTP1, MTP2 and MTP4, *L. major* MTP4 and members of the GH130 family, were aligned via the Cα atoms of the five-bladed

β-propeller structural motif using the structural alignment program MUSTANG v3.2.3 (Konagurthu et al., 2006). The structural alignment was used to compare the amino acids located in the Pi site, the −1 subsite and the +1 subsite (Table S2).

Man1P was manually docked into its putative binding site in the *L. mexicana* MTP4 crystal structure, using its location in the aligned GH130 family crystal complexes as a guide. GDP-Man and Man₈ were manually docked into their putative binding sites in the *L. mexicana* MTP1, MTP2 and MTP4 crystal structures so that the α-mannose portion of the molecules were in a similar location to that observed in the β-1,2-mannobiose:MTP2 (D94N mutant) crystal complex. Rotatable ligand torsion angles were adjusted manually as required to optimize the ligand interaction with nearby amino acid side chains. All manual manipulations were conducted using SYBYL-X 2.1.1. Each ligand, and any residues within a 6 Å radius of the ligand in the protein complex, was then geometrically optimized within SYBYL-X 2.1.1 using the same optimization protocol described above.

Models of eleven bacterial GT108 proteins identified in the evolutionary phylogenetic analysis of the MTPs (Figure S2; Table S3) and the nine characterized GT91 family members listed in the CAZy database (accessed on the 20th December 2018, http://www.cazy.org; Figure S5; Table S3) were constructed in an unbiased manner using the RaptorX structure prediction web server (http://raptorx.uchicago.edu/StructurePrediction/predict/) (Peng and Xu, 2011). For the bacterial GT108 proteins (Table S3), the optimal structural template selected by the RaptorX algorithm was *L. major* MTP4 (PDB: 2B4W). The GT91 proteins are predicted to be single pass type II membrane proteins comprising a short cytoplasmic domain, a helical transmembrane domain and a large extracellular domain. For eight of the characterized GT91 family members (BMT1_CANAL, BMT2_CANAL, BMT3_CANAL, BMT4_CANAL, BMT5_CANAL, BMT6_CANAL, BMT2_KOMPG and BMT3_KOMPG; Table S3), the largest region within the extracellular domain was predicted to be a five-bladed β-propeller. GT91 protein models were constructed using single, and also multiple, structural templates. The crystal structure of the GH130_1 family member MGP (PDB: 3WAS) was consistently selected as the single structural template for the highest ranked GT91 protein models, whereas lower ranked models used the crystal structures of Lin0857, RaMP1, RaMP2, BT3780 and *L. major* MTP4 (PDBs: 5B0P, 5YA9, 5AYD, 5A7V and 2B4W, respectively; Figures S2 and S5; Tables S2 and S3). The GT91 protein models constructed using multiple templates (all five-bladed β-propeller GH130 proteins) often had one slightly distorted or displaced blade, therefore structural comparisons with the *L. mexicana* MTPs were carried out using the GT91 protein models constructed from only the MGP template. Interestingly, one of the characterized GT91 proteins, BMT1_KOMPG, was predicted to be a six-bladed β-propeller and was excluded from the structural comparison with the *L. mexicana* MTPs. The PyMOL Molecular Graphics System, Version 2.1.0 (Schrodinger; https://pymol.org/2/), was used to visualize and analyze the protein structures and generate figure images.

Multiple Sequence Alignments and Phylogenetic Tree Building for the GT108 MTPs, and GH130 Proteins

The amino acid sequences of the seven *L. mexicana* MTPs and the homolog *L. major* MTP4 were aligned using ClustalΩ (as implemented in the MPI Bioinformatics Toolkit, https://toolkit.tuebingen.mpg.de/) (Zimmermann et al., 2018). The resulting multiple sequence alignment was then used as input to ESPript3.0 (http://espript.ibcp.fr/ESPript/ESPript/index.php) (Robert and Gouet, 2014; Edgar, 2004) to generate an annotated alignment (Figure S3).

For the phylogenetic analysis of the seven *L. mexicana* MTPs, ten bacterial GT108 proteins and eighteen characterized GH130 proteins, the amino acid sequences were aligned using MAFFT v7.0 (Katoh and Standley, 2013). The resulting multiple sequence alignment was used as input to ETE3 v3.0.0b32 (as implemented at GenomeNet, https://www.genome.jp/tools-bin/ete) (Huerta-Cepas et al., 2016) to construct the phylogenic trees. The ETE3 methodology used in the tree construction was PhyML v20160115 with model JTT (parameters: -f m–pinv e -o tlr–nclasses 4–bootstrap 100–alpha e) (Guindon et al., 2010). The branch supports were computed out of 100 bootstrapped trees. TreeDyn v198.3 (http://www.treedyn.org) as implemented on the Méthodes et Algorithms pour la Bio-informatique LIRMM web server (http://www.phylogeny.fr/one_task.cgi?task_type=treedyn) (Dereeper et al., 2008) was used to draw the unrooted tree (Figure S2A).

QUANTIFICATION AND STATISTICAL ANALYSIS

All values are the mean ± standard error using Excel and GraphPad Prism. All experiments were repeated at least twice and numbers of replicates, including the value of n in each experiment are indicated in the figure legends.

DATA AND CODE AVAILABILITY

The PDB accession codes for unliganded MTP1, unliganded MTP2, MTP2 in complex with mannose, MTP2 in complex with β-1,2-mannobiose and MTP4 in complex with phosphate anion, are PDB: 6Q4W, PDB: 6Q4X, PDB: 6Q4Y, PDB: 6Q4Z and PDB: 6Q5O, respectively.